DSTO

Source Localisation using Lloyd's Mirror Fringes on Narrowband Lines

Paul R. Lewis

DSTO-TR-0583

] APPROVED FOR PUBLIC RELEASE

DEPARTMENT ◆ OF DEFENCE
DEFENCE SCIENCE AND TECHNOLOGY ORGANISATION

Source Localisation using Lloyd's Mirror Fringes on Narrowband Lines

Paul R. Lewis

Maritime Operations Division
Aeronautical and Maritime Research Laboratory

DSTO-TR-0583

ABSTRACT

The analysis of the Lloyd's mirror interference of multiple narrowband lines from a sound source obtained with a single sensor is considered. A straightforward global least squares optimisation is discussed. The analysis is based on a straight line trajectory model of the source motion, and is configured for any range independent propagating medium. Two methods are proposed, each being based on a discrete optimisation on a predefined parameter grid. These are a simulated annealing algorithm and a guided search method. The least squares cost function is defined in a manner independent of the intrinsic shape of each narrowband emission. Simulation data based on an iso-speed sound profile are used to explore the proposed analysis.

Published by

DSTO Aeronautical and Maritime Research Laboratory
PO Box 4331
Melbourne Victoria 3001 Australia

Telephone: (03) 9626 7000
Fax: (03) 9626 7999

AR-010-366
October 1997

APPROVED FOR PUBLIC RELEASE

Source Localisation using Lloyd's Mirror Fringes on Narrowband Lines

Executive Summary

This report considers an approach whereby the interference patterns observed in lofargram (narrowband frequency-time plot) displays can be used to localise the range and depth of an underwater source. This is of significance since the approach is suitable in the analysis of separate independent lofargrams such as obtained from single sonobuoy sensors where otherwise no depth information can be obtained, and the range information is potentially highly uncertain. Having localised the source, the slant range can be used along with the measured time dependencies of the narrowband lines to estimate the absolute levels of the source over an extended azimuthal range. These in turn are required when estimating detection ranges for the source.

Lloyd's mirror interference patterns are often seen on lofargram plots and have been considered a nuisance when interpreting the data. The structure of these patterns however is intrinsically dependent on the range and depth of the originating source, and in principle can be used to extract these quantities. Whilst the source broadband levels are often too low to allow a fully developed pattern to be seen and analysed, the significantly higher level narrowband lines will also carry the interference modulation. We wish to extract and use the modulations from these narrowband lines.

The methodology advanced in the report is based on an iso-speed sound profile, although the extension to more realistic profiles is straightforward. We assume that the source moves with constant velocity and depth and that an approximate solution is known. Such a solution would typically include the CPA range and speed of the source obtained from a standard analysis of the narrowband lines, an estimate of the operating depth of the source and the sonobuoy depth setting. This defines a region of parameter space which along with a cost function is used to perform a multi-dimensional least squares optimisation. Because of the complex structure of the cost function we propose a suitable global optimisation strategy, and show that this is capable of extracting the required data. The end result is the extraction of the azimuthally dependent narrowband source levels.

Authors

Paul R. Lewis
Maritime Operations Division

Paul R. Lewis studied Nuclear Physics at the University of Melbourne, where he was awarded a PhD in 1990. He joined the Maritime Operations Division of AMRL in 1993 as a research scientist within the Submarine and Ship Sonar group in Sydney. He has since moved to the Torpedo Countermeasures group located at Maribyrnong in Melbourne, where he is developing torpedo encounter simulation models.

Contents

1. Introduction

In an earlier report [1] we considered how realistic, non-constant, sound speed profiles would affect the Lloyd's mirror interference pattern that can arise with moving sub-surface noise sources. Specifically, we were interested in utilising the information inherent in the interference pattern for source localisation using a single omni-directional sensor. Under the assumptions that the source is at a fixed depth and has a known constant speed, straight line motion, the resulting time dependent interference pattern allows an estimation of the source depth and range from the sensor. In that study the structure of the broadband intensity interference pattern evident in the time-frequency spectral plot (lofargram) was considered. The benefit of using the broadband interference pattern is the ease with which the frequency dependence of the interference fringe structure, which provides the clues to a unique estimation of the source-receiver relative position, can be incorporated into any position estimation.

The problem often arises, however, that no broadband interference pattern is visible in the lofargram. This may result from the source broadband emission being too weak, or from a weak reflected sound wave. As narrowband spectral lines can be significantly stronger than any broadband emissions, they may still exhibit interference effects, and thus be used to estimate the source position. In this case we have only a snapshot of the frequency dependence of the interference fringes at a few select frequencies. Although, ideally, data obtained at one frequency is sufficient to obtain an estimate of the source relative position, the inherent signal noise means that at least two well spaced frequencies are required if the position is to be determined with any accuracy. This report considers how these data might be used to provide such an estimation, and as a consequence, result in an absolute estimation of the signal strengths and beam emission patterns for any observed narrowband lines arising from the same source. It is these latter quantities that are of ultimate interest, as a knowledge of them is essential in determining detection probabilities for the source, or for source classification.

The aim of this work was to develop a tool for tertiary analysis of acoustic signatures, in which a simple computational approach to the analysis of narrowband line data could provide an estimation of the desired positional information. It might be possible to develop the tool into an operational aid for estimating the position of an acoustic source, in particular the depth of a submarine. The present paper examines the mathematical basis for such a tool, but does not consider the operational aspects. Realistic simulated data were used to test the tool as this enabled the true source parameters to be known and did not require this paper, which is essentially mathematical, to be classified. A limitation of this report is that the method has not yet been tested on real data. The generally poorer quality of and more complex structure in observed narrowband lines may restrict the suitability of approaches such as that proposed here to extracting any source localisation information intrinsically available.

2. Overview

We consider the situation in which a lofargram containing a number of narrowband lines is available. Ideally, this spectrum should be calibrated in magnitude, although this is not essential in the discussion to follow. It is assumed that any background contribution has previously been identified and calibrated in magnitude, and a (calibrated) frequency spectrum is available.

The source trajectory defines a range of aspects or "views" of the source as seen from the receiving position, where this view is the (sound) signal emission strength at a particular azimuth and elevation. As the source position changes, the strength of the received signal will vary in accordance with the signal strength at the associated azimuth and elevation angles, and with any spreading or propagation losses within the medium.

Over some time period about the time of the closest point of approach (CPA), each narrowband line will have some temporal line profile or shape, arising from the propagation loss and the source signal aspect dependence. Lloyd's mirror interference means that the received signal strength will result from a coherent combination of the emission strengths at two separate elevation angle values (for a fixed azimuthal angle), along with any reflecting boundary and propagation attenuation effects. Thus, in general, the strength of the received signal as a function of time will not be directly related to the source signal emission at any particular elevation angle, but will be the result of signals of differing intrinsic strengths coherently interfering, together with any attenuation and focusing effects of the propagation medium (as controlled by the sound speed variation). In turn, the source trajectory determines the specific mapping between the time and the source "view", and the degree to which the propagation medium will contribute. It is thus likely that an estimation of the source position at CPA (and hence for straight line motion, the trajectory) and the intrinsic source levels for a narrowband signal will be intractable without making acceptable simplifying assumptions, and being able to identify the origin of at least some of the observed signal strength variation. It is on this latter point that Lloyd's mirror interference can be of benefit, as the interference modulation of the narrowband line profile is often clearly identifiable by the approximately regular variation in the signal. The temporal positions of the minima due to this variation is strongly dependent on the geometry.

In the analysis to follow, a number of simplifying assumptions are made. The receiver depth is known. The source is taken to be travelling at a constant velocity, and at a constant depth. This reduces the source trajectory description to three parameters; the horizontal range at the closest point of approach (CPA range), the depth, and the speed. The medium is taken to be homogeneous, but with possibly a depth dependent sound speed. The reflection as described by a single reflection coefficient is taken to be frequency and angle independent. This assumption is reasonable for frequencies below a few kilohertz, at least for surface reflections at the water-air interface. The source sound emission (beam) pattern is taken to have only an azimuthal dependence. In the method to be discussed, this latter point primarily is only relevant for the

interpretation of the adjusted received signal strength, after interference and range effects have been removed, although a strong elevational dependence could affect the apparent placement of the interference minima. We limit ourselves to those narrowband lines with a sufficiently high signal to noise ratio. By "sufficient" we mean that the interference modulation is clearly identifiable above the random signal level fluctuations. Generally, this will be accomplished with a lower signal to noise ratio for strongly interfering sound waves than for weakly interfering sound waves since the interference pattern peak to trough height ratio will be larger. It is further assumed that we have prior knowledge of the source speed, the time of closest approach and the true frequencies of the narrowband emissions. Typically, these would be obtained from a Doppler analysis of the same narrowband line data.

The work discussed below is presented in terms of surface reflection in an infinite depth iso-speed medium. This is for convenience and does not restrict the application to either bottom bounce and non spherical spreading applications. In principle the modelled loss data can arise from an analytical expression as used here, or from direct numerical evaluation. No attempt has been made, however, to assess the degree to which a non-constant sound speed profile will complicate the analysis. This is an area for future work.

The basic approach to the source localisation solution is to recognise that the Lloyd's mirror interference essentially results in a modulation of the received signal line profile. Considering the iso-speed propagation model, the received intensity for two ray interference is given as

$$\begin{aligned} I &= \frac{I_D}{R_D^2}\left(1+\eta^2\frac{I_R R_D^2}{I_D R_R^2}+2\eta\sqrt{\frac{I_R}{I_D}}\frac{R_D}{R_R}\cos\left(\frac{2\pi f}{C_S}(R_R-R_D)+\phi_0\right)\right) \\ &= \frac{I_D}{R_D^2}\left(1+\gamma^2\frac{R_D^2}{R_R^2}+2\gamma\frac{R_D}{R_R}\cos\left(\frac{2\pi f}{C_S}(R_R-R_D)+\phi_0\right)\right) \qquad \text{where} \quad \gamma \equiv \eta\sqrt{\frac{I_R}{I_D}} \end{aligned} \tag{1}$$

where I_D (R_D) and I_R (R_R) are the direct and reflected wave intensities (path lengths), f is the line frequency, C_S is the (constant) sound speed, η is the reflection coefficient and ϕ_0 is the phase shift arising from reflection at the boundary. Thus, the received signal appears as approximately the expected direct wave signal intensity, modified by a frequency and time dependent function of the source CPA range, depth and speed. Notice that the azimuthal and elevational dependence are subsumed into the effective reflection coefficient γ, which correctly will not be constant in time unless the source signal beam pattern is isotropic in nature. However, because we have explicitly removed the propagation range dependence, it will remain nearly constant over some suitable time interval about the CPA time.

Therefore, for any number of possibly harmonically related narrowband lines originating from the same source, the received signal intensities can be separated into the product of an intrinsic component times a "common" component. The latter

contains the information concerning the source position, so that a direct estimation of the source trajectory based on any number of narrowband line profiles is possible. We indicate the "common" component as such because it is frequency dependent, however this dependence is calculable once a model of propagation is assumed.

The problem as now cast is to identify the "common", or interference modulation, pattern in the narrowband line data and remove the intrinsic component of each line profile, leaving a set of data that apart from the line frequency, depends on the same set of parameters. A global search parameter estimation can then be performed to provide an estimate of the underlying source trajectory. Without any further information we will assume that the data are normally distributed random quantities, in which case the least squares estimator provides the minimal unbiased estimate of the solution point.

As indicated, it is taken that the source speed, time of CPA and line frequencies are known. If it is assumed that there is no elevational dependence of the source beam pattern, the reflection coefficient η will be constant for all lines. Thus, a global search in our model will require the identification of three parameters; the source CPA range and depth, and the reflection coefficient. The small number of parameters makes feasible a grid search or evaluation over a defined region of parameter space. In particular, if the determination of the reflection coefficient can be decoupled from the estimation of the source CPA range and depth, the problem is well suited to such an approach. Ideally, this is the case as the source-receiver geometry defines the positions, and the reflection coefficient the strength of the interference modulation minima. The introduction of noise and a non-isotropic beam profile will alter this. If, as would be most likely, the source speed, CPA time and line frequencies are derived from a Doppler frequency shift analysis, an estimate of the CPA range will also be obtained. The accuracy of such a range will generally not be high, however it can be used in determining a possible search grid size and position. The cost function to be defined in §2.3 effectively decouples the reflection coefficient from the source CPA range and depth parameters, so we consider here how these latter two quantities may be determined.

As the aim is to be able to include any range independent propagation loss model, we need to be able to include efficiently general propagation loss data into the calculations. A typical propagation loss programme would provide as the minimal output the calculated loss as a function of horizontal separation distance, for an isotropically radiating source of unit strength (ie. 0 dB loss at 1 m separation) at specified source and receiver depths. Basing any parameter search, at least in the first instance, on a grid allows such data to be directly incorporated in a reasonably efficient manner. For a given receiver depth, at each source depth on the search grid, the loss data need only be calculated over the horizontal ranges

$$R_{MIN} = R_{CPA}(\min)$$
$$R_{MAX} = \sqrt{R_{CPA}(\max)^2 + (V \cdot \Delta t(\max))^2} \qquad (2)$$

where V is the source speed and Δt is the time from CPA, to encompass all the grid CPA range values.

This suggests that the calculations proceed in three steps: a region of valid parameter space is defined and a search grid is constructed, the propagation loss data is calculated for each source depth point on the grid over the range limits set in equation 2, and the cost function is evaluated at the discrete grid points such that the position of the global minimum is found.

In the method to be suggested, this approach is used as an initial estimation of the solution point, after which a refined value is obtained.

2.1 Parameter grid determination

A typical loss curve for Lloyd's mirror interference will have three regions; the near field, the interference field, and the far field. In the interference region, the loss will oscillate in a roughly periodic manner. Both the source depth and the CPA range will effect the placement of the interference region. As either of these parameters is varied, the phase difference between the direct and reflected waves will also vary, and the loss will fluctuate from one local extremum to the next (eg. from a local maximum to a local minimum). The step sizes then must be selected such that the change in phase remains less than π radians. Otherwise, aliasing of the sampled loss data will occur.

The variation in loss derived for the iso-speed propagation model serves as the basis for determining this spacing. From the equation giving the received signal intensity for two ray interference, with $I_D = I_R = I_0$,

$$I = I_0\left(\frac{1}{R_D^2} + \frac{\eta^2}{R_R^2} + \frac{2\eta}{R_D \cdot R_R}\cos(\phi + \phi_0)\right) \quad \text{with } \phi = k(R_R - R_D),\ k = \frac{2\pi f}{C_S} \tag{3}$$

the variation in loss from a local maximum to local minimum will occur over a range ΔR such that $\Delta\phi = \pi$. Expressing the ranges in terms of the CPA range R_0 and the source and receiver depths D_S and D_R respectively, we have for surface reflections

$$\begin{aligned} R_R &= \sqrt{R_0^2 + (D_S + D_R)^2 + (V \cdot \Delta t)^2} \\ R_D &= \sqrt{R_0^2 + (D_S - D_R)^2 + (V \cdot \Delta t)^2} \end{aligned} \tag{4}$$

whence we obtain the partial derivatives

$$\frac{1}{k}\frac{\partial\phi}{\partial D_S} = \frac{\partial\phi}{\partial R_R}\frac{\partial R_R}{\partial D_S} + \frac{\partial\phi}{\partial R_D}\frac{\partial R_D}{\partial D_S} = \frac{D_S + D_R}{R_R} - \frac{D_S - D_R}{R_D}$$
$$\frac{1}{k}\frac{\partial\phi}{\partial R_0} = \frac{\partial\phi}{\partial R_R}\frac{\partial R_R}{\partial R_0} + \frac{\partial\phi}{\partial R_D}\frac{\partial R_D}{\partial R_0} = \frac{R_0}{R_R} - \frac{R_0}{R_D} \qquad (5)$$

For reflections from a bottom layer at a depth Z_0, (D_R+D_S) is replaced with $2Z_0-(D_R+D_S)$ in equations 4 and 5. Putting

$$\Delta D_S = \left(\frac{\partial\phi}{\partial D_S}\right)^{-1}\Delta\phi$$
$$\Delta R_0 = \left(\frac{\partial\phi}{\partial R_0}\right)^{-1}\Delta\phi \qquad (6)$$

with $\Delta\phi = \pi$ gives the conditions for the maximum step sizes as

$$\Delta D_S \le \frac{C_S}{2f_0}\left[\frac{D_S + D_R}{R_R} - \frac{D_S - D_R}{R_D}\right]^{-1}$$
$$\Delta R_0 \le \frac{C_S}{2f_0}\left[\frac{R_0}{R_R} - \frac{R_0}{R_D}\right]^{-1} \qquad (7)$$

Recall that R_R and R_D are functions of the two parameters, R_0 and D_S. The variation in the maximum depth and range increments is shown in figure 1 for $D_R = 100$ m and $f_0 = 150$ Hz. Equation 7 shows that the required grid size (number of elements) increases as the square of frequency.

In producing a regular parameter grid for a number of narrowband lines, we need to select, for the maximum line frequency, the ΔD_S and ΔR_0 which define the minimum along the surfaces in figure 1. The heavy contour lines shown therein indicate the appropriate step sizes. Values for D_S and R_0 can be determined iteratively as follows.

Starting at the smallest source depth, a sequence of source depths is firstly generated by setting

$$\left.\frac{\partial\kappa}{\partial R_0}\right|_{D_S = \text{Const}} = 0 \quad , \quad \kappa \equiv \frac{\partial\phi}{\partial D_S} \qquad (8)$$

and solving for R_0. This will give the largest κ (the smallest step size) for the specified fixed D_S. The estimated value for R_0 is then used to produce a new D_S value from equation 7a and the procedure is repeated. The contour of the minimum ΔD_S and a sequence of source depths is thus produced.

The R_0 steps are estimated at the calculated sequence of source depth values from equation 7b by calculating the increase in R_0 at each of the source depths and selecting the minimum value. This leads to the next value for R_0 and the procedure is repeated. Thus, a regular grid built from the minimum step sizes is generated.

In practice, the step size should be smaller than that produced from equation 7. The values therein give the maximum sizes to prevent aliasing for the iso-speed propagation model, however for a non-constant sound speed profile, the loss can be expected to vary over a smaller range [1]. Because of this, the only sure way of ensuring that the grid spacing is sufficiently small is to actually evaluate the loss over the grid and monitor the spacing between loss maxima and minima. The grid spacing must be small enough to see this structure.

2.2 Loss data determination

According to the above scheme, the loss data are evaluated at the parameter grid source depth values, and over the horizontal ranges identified in equation 2. For a given CPA range (and known source speed and CPA time), the time values of the experimental narrowband line data will define the ranges at which the loss data must be evaluated. The required values can be correctly evaluated from tabulated loss values at specific ranges as long as the tabulated range step sizes are sufficiently small to allow interpolation. Thus, we choose the range increments for each given D_S value so as to prevent the aliasing of the loss data. We follow a similar method to that for the selection of the R_0 values, but now use

$$\frac{1}{k}\frac{\partial\phi}{\partial R} = \frac{R}{R_R} - \frac{R}{R_D} \quad \text{where} \quad R = \sqrt{R_0^2 + (V\cdot\Delta t)^2}$$

and

$$\Delta R \le \frac{C_S}{2f_0}\left[\frac{R}{R_R} - \frac{R}{R_D}\right]^{-1} \tag{9}$$

to evaluate the increment in the horizontal range, R, at each source depth value.

Again, the step size should be smaller than the above estimation. When sufficiently small this then allows linear interpolation of the calculated loss values to be used when estimating the loss at the ranges implied by the experimental times.

2.3 Least squares cost function

The critical component of a least squares optimisation is in the definition of the cost function to be minimised. The problem in the current situation is that we wish to constrain the search to match specific features of the experimental line profile data, viz. the Lloyd's mirror component of the signal level. In general it can be expected that the received signal will not be symmetric about the CPA time. Further, the measured signal will always have an attenuation arising from the spreading loss. It must be

assumed that there is no a priori knowledge of the shape of the source beam pattern. The feature here of importance is the positioning of the Lloyd's mirror interference fringes. Thus, we need to separate the signal variation into that arising from the source beam pattern, ie. the attenuated intrinsic signal, and the interference modulating pattern. Having achieved this, the parameter estimation can be performed using the modulating function alone.

It is not sufficient to directly use the measured line profile in the parameter estimation. The non-symmetry and spreading attenuation of the signal will introduce a bias to the parameter estimation as the sum of squares will be sensitive to the overall shape of the line profile.

To perform a separation of the intrinsic and modulation components, it is observed that typically the temporal variation of the interference fringes will be faster than the variation of the intrinsic signal (excluding the random noise variation). The interference fringes will appear as a pseudo periodic signal in many cases. A simple rectangular running average filter of an appropriate width can then be employed to achieve the separation. The filter window size must be chosen according to the "periodicity" of the interference fringes, and will differ with each frequency. To handle the edge effects of such a filter, the filter width is made to reduce as the extremities of the data sequence are approached. In these regions the filtering will not be as suitable, however, owing to the spreading attenuation, the importance of these regions to any sum of squares function can be reduced.

The most straightforward approach to determining the filter width at each frequency is from a manual evaluation of the positions of the interference fringes. In the process to be discussed herein, it is assumed that the positions of the interference fringe minima are identified prior to processing. That this can be done is guaranteed by the earlier assumption that the interference fringes are clearly identifiable. Knowing the approximate fringe spacing, a filter width set at some multiple of this spacing will be adequate.

Applying such a filter to the line profile data will generate an estimate of the received intrinsic line profile. This estimate will improve as the interference modulation better approximates a periodic function. Having an estimate of the received intrinsic line profile, the interference modulation function is directly extracted from the data. This modulation function will be independent of the source beam pattern and any spreading attenuation, and the ratio of the peak to trough heights will be directly dependent on the degree of reflection.

The effect of applying a running average filter to various interference modulated line profiles is shown in figure 2. A window width approximately four times the interference (temporal) fringe spacing has been selected. This value is found to adequately reproduce the underlying intrinsic beam profile. Because of the attenuation of the signal with the time from the CPA, T_0, smoothing the raw signal will introduce a bias and overestimate the signal at large time offsets. This will become more

pronounced as the filter width is increased. Using the logarithm of the raw data will reduce the variation in signal strengths over the filter window, and thus the smoothing filter will lead to a better estimate of the true attenuated signal strength. Figure 2a shows the effect on the estimated attenuated intrinsic line profile of such a filter, along with the true line profile shape. The modulation functions are shown in figure 2b. This shows that where the interference fringes lack a strong periodicity, the beam profile estimation is inadequate. The representation of the signal at times close to T_0 depends on the phasing between the direct and reflected sound waves. For destructive interference, the signal, and thus the modulation function, is underestimated. This should have little effect on the parameter estimation as the positions of the fringes in the modulation function are the critical factor in determining the source position and the central region will represent only a small part of the entire modulation function. Likewise, the estimation of the effective reflection coefficient will be determined from the overall variation in the modulation function, and thus any underestimation should have a minor effect on the deduced value.

An example is shown in figure 3 for three frequencies for which the phase at T_0 varies between 0 and π. An isotropically radiating source was assumed, with a CPA range of 477 m, source and receiver depths of 50 and 200 m respectively, and a source speed of 5 m/s. The difference between the actual and the estimated signal profiles depends somewhat on the width of the filtering window and the size of the reflection coefficient, η, but for destructive interference, varies between two and four decibels for the above geometry where $0.1<\eta<1.0$ and the filter width is between 100 and 200 seconds.

Following from the definition of equation **1**, we define the interference modulation function for a frequency f_i as the time dependent loss at a specific line frequency corrected for the spreading loss. Thus, for spherical spreading we have

$$F_M(i) = 1+\gamma^2\frac{R_D^2}{R_R^2}+2\gamma\frac{R_D}{R_R}\cos\left(\frac{2\pi f_i}{C_S}(R_R-R_D)+\phi_0\right) \qquad \textbf{(10)}$$

This contains the (assumed constant) effective reflection coefficient γ. The least squares cost function is defined in terms of this function, and the received signal level Ψ_E as

$$C_f = \sum_{data} W(i)\cdot\left(\sigma_E(i)-\sigma_T(i)\right)^2$$

with $$W(i) \equiv \frac{\overline{\Psi}_E(i)}{\max\left\{\overline{\Psi}_E(i)\right\}}\,,\quad \sigma_E(i) \equiv \left|\frac{\Psi_E(i)}{\overline{\Psi}_E(i)}\right| \quad \text{and} \quad \sigma_T(i) \equiv \left|F_M(i)\right| \qquad \textbf{(11)}$$

In this equation the double bars ($|G|$) indicate that the enclosed quantity is normalised with

$$|G(i)| = \frac{G(i)}{\sum_{data} G_j} \quad \text{for function G} \tag{12}$$

This is done as only the shapes of the experimental and modelled line profiles are of interest. The barred ($\overline{G}$) quantities represent the filtered line profile data. Thus, σ_E is an estimation of the Lloyd's mirror modulation function.

To include numerically evaluated loss data, the modulation function F_M would be replaced by the calculated loss data, but this still requires the direct ray spreading loss correction. In the current case we have chosen to approximate this with the spherical spreading correction appropriate for an iso-speed medium. A model dependent form for the spreading loss experienced by a single direct ray could be evaluated numerically, however, correctly, this would need to be done at each range implied by the current parameter set.

Each datum point in the summation of equation 11 is weighted according to the relative strength of the estimated received intrinsic signal using the weighting function W. This reduces the importance of the lower signal to noise sections of the data.

When multiple lines are being considered concurrently, each narrowband line will generate a sum of squares value as defined above, and the total cost function is defined as the geometrical mean of the individual values, giving

$$C = \left(\prod_{freq} C_f \right)^{\frac{1}{N}} \quad \text{for N frequencies} \tag{13}$$

In this way no single line is permitted to dominate the parameter selection unduly, and a fit that adequately represents all the data is obtained. This is appropriate as multiple narrowband lines are required for a well defined solution.

3. Parameter Estimation

Without further information, an unconstrained non-linear least squares estimation of the parameters is necessary. Figure 4 shows the cost function evaluated for a single narrowband line over a region of parameter space surrounding the known solution point. The data are the result of a simulation in which an isotropically radiating source is modelled. The simulation geometry has a source depth of 50 m, a CPA slant range of 500 m, a receiver depth of 200 m and a reflection coefficient is 0.5. The source narrowband line frequency is 150 Hz. Evidently the cost function has a complex structure, consisting of multiple valleys and local minima. The valleys represent regions of approximately constant phase difference between the direct and reflected sound waves. The correct solution point is identified from this plot, however the

identification of this point through a function minimisation parameter search would be critically dependent on the starting point. A suitable point will not be known in advance. With a frequency independent medium the length of features on the cost surface will scale inversely with frequency. Thus, the higher the frequency, the closer the initial point needs to be to the solution point in order that a successful parameter estimation is obtained.

Two approaches may be taken in order to overcome this. A statistical search of the cost function minimum can be performed using a technique such as a simulated annealing algorithm. This provides a constrained random walk through the parameter space, searching for the global minimum. A simulated annealing parameter estimation requires no gradient information, however the estimation can become expensive in terms of the number function evaluations that must be made. Such an approach can be readily applied to a discrete parameter space such as is constructed herein and an algorithm is discussed further in appendix A. The suggested algorithm is found to successfully identify the global minimum for the simulation cases considered in this section. Other statistical searching methods such as genetic algorithms also may be suitable, but have not been considered.

A second approach is a guided search in which the solution region of the parameter space is localised by the direct evaluation of the cost function on a grid, leading to the selection of an appropriately close initial point. An unconstrained direct non-linear parameter search can then be performed in the confidence that the estimation will converge to the correct solution point.

In both cases, an initial region of parameter space must be defined. A Doppler solution to any of the narrowband line frequency shifts will produce source speed and CPA range estimates. Of these, the range value will usually be the least well defined as it is governed by the rate of change in the Doppler frequency with time, but may prove useful in providing loose bounds on the CPA range solution point. No information concerning the source depth can be gleaned from a Doppler analysis, and either an estimate based on other information or a scan of the parameter space will need to be made. The automatic search capacity of the simulated annealing algorithm allows a generously sized parameter space to be assumed, albeit potentially at the expense of a large number of cost function calculations. However, with the present methodology, these calculations still require the pre-calculation of the propagation loss data, and this may be the limiting factor in deciding the size of the parameter space and the resolution of the search grid. Certainly, with a large parameter grid the simulated annealing optimisation would require far fewer cost function evaluations than a full evaluation of the grid.

For the guided search, and without further information, the cost function will need to be evaluated over an arbitrarily positioned low resolution parameter grid, and the regions of local minimum identified. In doing this, it is better, following the reasons outlined below, to consider the total cost function. The higher frequency data, in particular, are important. Because the number of grid points increases as the square of

the highest frequency, even with a coarse grid step size (eg. near to the limits defined in equation 7) the number of cost function evaluations may become large and a compromise between the size of the parameter space, resolution and the maximum frequency will have to be made. After candidate solution points have been located, these may require a closer inspection at a higher resolution so as to ascertain whether a reasonable solution point (the CPA range and source depth) is exposed. The suitability of a candidate solution point can be obtained by evaluating the modulation functions for each of the narrowband lines. If the point is incorrect, the match with the data will become increasingly worse as the line frequency differs from the frequency used in deriving the estimation. This is a faster method than evaluating the total cost function, which, depending on the range of frequencies, may require a large number of grid points, leading to a heavy computational and memory demand.

After a suitable region of parameter space has been isolated and a starting point is identified, the parameter search should include all suitable narrowband line data. The search does not need to be constrained to discrete parameter values at this point. It is important for two reasons to use the total cost function defined in equation 13. The individual modulation functions, and hence the estimate of the source position, will be increasingly more sensitive to variations in the source-receiver geometry as the narrowband line frequency increases. Secondly, the total cost function displays a more simplified structure than do the individual functions defined by equation 11. Using the above simulation geometry, figure 5 shows the total cost function evaluated for six narrowband lines with frequencies between 50 and 750 Hz. The solution point is clearly identified, but is also very localised in parameter space. The relative flatness of the surface in comparison to figure 4 arises because apart from the position of the minimum at the true solution point, the positions of the various structures on the surface are frequency dependent. With multiple narrowband lines, the variations in the individual cost functions tend to cancel except at the true position where all contribute towards a minimum value.

It should be emphasised that the method described in this report generally would require a number of spaced frequency lines to generate a well defined solution. As the signal to noise ratio of the data increases, the number and frequency range required for such a solution would reduce (eg. with ideal data, only a single narrowband line would be necessary to define the source - receiver geometry). No assessment of the limitations imposed by differing signal to noise ratios has been made.

In the above, we have assumed that a suitable reflection coefficient is being used. The next section discusses how the dependence of the cost function on the reflection coefficient can be decoupled from that for the source depth and CPA range. Therefore, as the size of the interference fringes is directly dependent on the degree of reflection, we can estimate a value directly from the strengths of the modulation functions. Using the iso-speed model, the bounds on the strength of the modulation function at each frequency can be calculated, and by adjusting the reflection coefficient, these can be made to best represent the strengths of the modulation functions for each of the

narrowband lines. An example is shown in figure 6 for some of the same simulation data used in figure 5.

3.1 Narrowband analyses

We consider two Lloyd's mirror narrowband line analyses of simulated data. This allows a model consistent with the assumptions outline above to be studied. The source travels at constant speed in a straight line, and at a fixed depth. The received signal is the result of two beam interference between a direct and a surface wave with the surface boundary having a constant reflection coefficient of 0.5. For simplicity, the propagating medium has a constant sound speed. The narrowband line signal to noise ratios are chosen such that interference pattern is clearly identifiable.

A simplified source beam pattern with only an azimuthal dependence is modelled. Thus, the direct and reflected beams have the same intrinsic strength, and the estimated source beam pattern can be directly compared with the true beam pattern. The estimated beam pattern is the result of the direct division of the measured line profile by the fitted modulation function and, correctly, is the true beam pattern in this case. We take the azimuthal dependence to be a sum of Legendre polynomials,

$$I_0(\theta,\phi) = \left(\sum_{L=1}^{3} \alpha_L P_L(\cos\theta) \right)^2 \qquad (14)$$

where the L=2 and L=3 terms represent an asymmetric forward–aft dipole pattern. The two cases to be considered include a symmetric and asymmetric forward-aft pattern.

The source and receiver depths are 50 m and 200 m respectively. The slant range at CPA is 500 m, and the source speed is 4.9 m/s. Six narrowband lines are considered; at 50, 150, 300, 400, 550 and 750 Hz. Figure 7 shows the positions of the broadband interference minima fringe contours and these narrowband lines. The frequencies are selected so as to include a differing number of interference minima. All source frequencies have the same emission beam pattern, with this being either of two choices. The symmetric pattern is constructed using equation 14 and the coefficients (α_1, α_2, α_3) = (1.0, 0.0, 0.75), whilst the asymmetric pattern uses the coefficients (α_1, α_2, α_3) = (1.0, 0.5, 0.75). The emission beam patterns for these coefficients are shown in figure 8. For clarity we assume that the source does not emit any broadband signals. Thus, the received signal comprises the tonals and a broadband background noise.

Using the above parameters, a digitised time series of the received signal is constructed [2], and the narrowband data are extracted using the programme AMADEUS [3]. For the present purposes the narrowband data in the form of received signal strength at each time step are required.

The received signal strengths as a function of time, and with the background contribution removed, are shown in figures 9a and 9b for the two beam emission patterns, from which the interference fringes are clearly identifiable. The purple and red curves on these plots respectively indicate the estimated and true received intrinsic strengths based on a filter width of four. The 50 Hz data has one node either side of the time of CPA, and the filter produces a poor estimate of the true shape. The 150 Hz data has two nodes, and the filter produces a result which is marginal. This is more clearly shown by the extracted modulation functions in figure 10. The lower and upper bounds, evaluated for straight line propagation and a reflection coefficient of 0.5, are included on these plots. With correct filtering, the two modulation functions should be similar, and vary between these limits.

Equation 11 includes an optional weighting function which biases the cost function towards the strongest parts of the received narrowband line profiles. The effect of this factor on the ability of the cost function to correctly locate the solution point is shown in figure 11. This shows the individual cost functions, evaluated using the correct reflection coefficient of 0.5, for the symmetric and asymmetric beam profile 150 Hz data sets respectively. The independence of the cost function on the form of the source beam pattern is evident. The unweighted cost function exhibits a significantly more structure than the weighted function, and many potential solution points. Indeed, in this example the location of the minimum value on the grid is considerably removed from the correct position. When the weighting is applied, the structure of the cost function is considerably simplified, and the correct solution point is identified. The effect on the total cost function is less pronounced because of the averaging done in producing this value.

Parameter estimations based on the total cost function evaluated with and without data weighting indicate that the weighted estimations produce consistent (and correct) values for the source depth and CPA range, independent of the value of the reflection coefficient. If the reflection coefficient is also varied, the weighted estimation also produces the correct value for this quantity. Without weighting the estimated solution point depends on the chosen value for the reflection coefficient. Further, when this coefficient is allowed to vary, values dependent on the initial value of the reflection coefficient are obtained.

It appears that the weighting of the data is useful for two reasons. The structure of the individual cost functions is simplified, which improves the selectivity of the starting point for any search, and the dependence of the cost function on the source depth and range at CPA is better decoupled from the boundary reflection coefficient. This separation is of advantage to both optimisation methods as the reflection coefficient can be estimated from the modulation function without the need for a three dimensional search. In particular, it is useful for the guided search where a good initial point must be defined. Then, a nominal value for the reflection coefficient can be assumed (eg. 0.5 or some estimate based on the strength of the modulation function) whilst a suitable initial source depth and range are determined. A concurrent optimisation of these three parameters can then be performed.

Parameter correlations are shown in figures 16 and 17, wherein the source depth and the range at CPA are seen to be strongly correlated. The correlation between these parameters and the reflection coefficient is weaker because they will be primarily sensitive to different features of the modulation function (viz. the fringe positions and the fringe peak to trough variation respectively). The weighting of the data presumably simplifies the cost function structure and better separates the dependence on the parameters because it biases toward the data about the time of CPA where the interference modulation will be clearest. The data at times far from CPA will be less affected by the interference modulation, especially after the last interference minimum, and, with the signal being weaker, will be more susceptible to the influence of noise.

The global optimisation fits to the various line profiles are shown in figure 12. Using these model curves, estimates of the source emission patterns can be extracted, and are shown in figure 13. The emission patterns can then, under the assumption of a purely azimuthal dependence, be analysed in terms of the three term Legendre sum of equation 14 to produce an analytical beam pattern.

The simulated annealing algorithm applied to these same simulations provides a direct estimate of the solution point. Considering only the weighted cost function, the algorithm correctly identifies the modelled source depth and CPA range. Three runs were made in which surface reflection coefficients of 0.25, 0.50 and 0.80 respectively were assumed. A large parameter space with a medium resolution grid was used. The sampled total cost function surface is shown in figure 14 for the data with a reflection coefficient of 0.5. The sampled cost function shows how the annealing algorithm concentrates on the region of the solution point, but also widely samples the parameter space. The evolution in the annealing process is shown in figure 15. The number of sampled parameter configurations for the symmetrical dipole beam pattern was 1906 with the annealing requiring 13 cycles. Following the discussion in appendix A, the hit rate was 2.1% leading to 1866 separate function evaluations, or 2.2% of the full parameter grid. Such statistics are dependent on the size if the parameter grid. The present size was 315×274.

4. Uncertainty analysis

There are two aspects to the estimation of the uncertainties in the deduced parameters. The optimisation is performed with the assumption that the source speed, time of CPA and receiver depth are known. The stability of the solution point to these needs to be established. Of these, the receiver depth and time of CPA should be well known. The speed may be less so, with this depending on the strength of the narrowband lines under analysis. Secondly, an estimate of the uncertainty in the least squares parameters arising from the quality of the fit needs to be determined.

As the functional dependence of the location of the minimum in the cost function is unknown in general, and because it will certainly have a non-linear dependence, the easiest way of assessing the dependence of the solution point on the source speed,

receiver depth and the time of CPA (V, D_R, T_0) is with a numerical variational analysis. For the special case of a iso-speed medium, an analytical expression relating the dependence can be derived. The iso-speed case does not produce a unique solution point, as can be shown from a consideration of the expressions for the phase, equation 3, and the path lengths, equation 4. Thus, we have with rearrangement,

$$\begin{aligned} \phi &= k\cdot(R_R - R_D) \\ R_R &= \sqrt{(R_0^2 + V^2\Delta t^2)}\sqrt{1+\frac{(D_S + D_R)^2}{R_0^2 + V^2\Delta t^2}} \\ R_D &= \sqrt{(R_0^2 + V^2\Delta t^2)}\sqrt{1+\frac{(D_S - D_R)^2}{R_0^2 + V^2\Delta t^2}} \end{aligned} \qquad (15)$$

which, making a first order Taylor's expansion of the path lengths, gives

$$\begin{aligned} \phi(t=T) &= k\cdot(R_R - R_D) \\ &\approx \tfrac{1}{2}k\sqrt{R_0^2 + V^2\Delta T^2}\left\{\frac{(D_S + D_R)^2}{R_0^2 + V^2\Delta T^2} - \frac{(D_S - D_R)^2}{R_0^2 + V^2\Delta T^2}\right\} \\ &= \frac{2kD_SD_R}{\sqrt{R_0^2 + V^2\Delta T^2}} \quad ,\Delta T \equiv T - T_0 \text{ and } \frac{(D_S + D_R)^2}{R_0^2 + V^2\Delta T^2} << 1 \end{aligned} \qquad (16)$$

Then, when the phase is held constant at ϕ_0 the approximate expression

$$V = \frac{R_0}{\Delta T}\left[\left(\frac{2kD_SD_R}{\phi_0 R_0}\right)^2 - 1\right]^{\frac{1}{2}} \qquad (17)$$

defines the relationship between the source speed, depth and CPA range, and the receiver depth for a constant phase at each time step, and therefore a constant modulation function. A non-unique solution point is also expected [1] with a non-constant sound speed profile.

In the present case V, D_R and T_0 can be assumed to be independent, and the scatter in their values will imply a scatter in the solution point. The independent uncertainty bounds on the source depth, range at CPA and reflection coefficient can then be determined. Such an analysis will be computationally intensive in that a least squares optimisation starting from the same initial point needs to be performed for each triplet of known values, and the set of triplets needs to be sufficiently large that the range of each quantity is well sampled.

The stability of the solution point in the example discussed in §3 is considered. To do this the assumed constant receiver depth, time of CPA and source speed were taken as normally distributed quantities with 2σ levels (mean values) of 3 (200) m,

1 (385) seconds and 0.75 (4.9) m/s respectively. The solution points for the CPA range, source depth and reflection coefficient were determined for a sample of 80 configurations drawn from these distributions. The results are shown in figures 16 and 17.

The expected strong positive correlation between the deduced CPA range and the source depth is observed, whilst no correlation between the reflection coefficient and these quantities is found. The magnitude of the variations in the source depth and CPA range is consistent with equation 17. The independence of the reflection coefficient is expected as the phase difference between the direct and the reflected sound waves is independent of the reflection coefficient. The origin of the strong correlation is the source speed. The scatter in the deduced source depth values with the variation in the source speed is presumed to arise (equation 17) because of the concurrent independent variation of the receiver depth. A particulary definite relationship between the source speed and the deduced CPA range is noted.

The resultant CPA ranges and source depths are normally distributed about the expected mean positions (482 cf 477 m and 50.7 cf 50 m), with 2σ levels of 76 and 6.9 m respectively. Clearly, the least squares solution point is sensitive to the source velocity. Any accurate estimation of the source trajectory therefore demands that this quantity, in particular, is well defined, as equation 17 indicates approximately equal fractional uncertainties for the source depth, CPA range and the source speed.

Given an estimate of the solution point, an estimate of the least squares uncertainty in this should be established. Owing to the non-linearity of the problem, only an approximate estimate of the uncertainties can be made. The cost function surface shows the correlation between the source depth and range at CPA, for all other parameters fixed. A contour of constant value (or a surface when three parameters are considered) about the solution point indicates an uncertainty bound on the solution point. The confidence level to be assigned to any contour requires a knowledge of the probability distribution of the data. Assuming a χ^2 distribution, the confidence level can be calculated from the F-distribution. Thus, the contour level associated with a confidence level of $(1-\alpha)$, $C(\hat{\theta},1-\alpha)$, is

$$C(\theta,1-\alpha) = C(\hat{\theta})\left\{1+\frac{p}{n-p}F(p,n-p,1-\alpha)\right\} \qquad (18)$$

where $C(\hat{\theta})$ is the magnitude of the cost function at the solution point and $F(p, n-p, 1-\alpha)$ is the F-distribution for p variables, (n–p) degrees of freedom and a confidence level of $(1-\alpha)$.

An alternative, simpler, approach is to linearise the problem. Then, the confidence levels appropriate for a linear least squares optimisation can be used. In summary, the data Y are assumed to be represented by the model function $F(\xi,\theta)$ which, using Taylor's theorem, is expanded about the solution point giving

$$F(\xi_u,\theta) \approx F_u^0 + \sum_{i=1}^{p} Z_{i,u}^0 \cdot (\theta_i - \hat{\theta}_i)$$

with $$F_u^0 = F(\xi_u,\hat{\theta}) \quad \text{and} \quad Z_{i,u}^0 = \left.\frac{\partial F(\xi_u,\theta)}{\partial \theta_i}\right|_{\theta=\hat{\theta}_i} \tag{19}$$

In equation 19 the $\hat{\theta}$ are the best estimates of the parameters θ, F^0 is the value of F evaluated at the solution point and the Z^0 are the linear coefficients. Each of these is evaluated at the data points ξ_u. Thus, the fitting function is

$$(Y - F_u^0) = \sum_{i=1}^{p} Z_{i,u}^0 \cdot (\theta_i - \hat{\theta}_i) + \varepsilon_u \tag{20}$$

The linear least squares uncertainty estimate is obtained from $(\mathbf{Z}^T\mathbf{W}\mathbf{Z})^{-1}$ where $\mathbf{Z}$ is the n×p matrix (n data points×p parameters) formed from the $Z_{i,u}$ and W is a diagonal weight matrix. Assuming that the χ^2 distribution is appropriate, the independent uncertainties $\delta\theta_i$ are obtained from the diagonal elements of the covariance matrix

$$\mathbf{C}_V = (\mathbf{Z}^T\mathbf{W}\mathbf{Z}) \cdot S^2 \cdot t(n-p, 1-0.5\alpha)^2$$

giving $$\delta\theta = \sqrt{\text{diag}(\mathbf{C}_V)} \tag{21}$$

where S^2 is the data variance and the t(n-p,1–0.5α) is the Students t-value for a confidence level of (1–α).

The variance is estimated from a sum of squares (SS) analysis, using

$$SS_{TOTAL} = SS_{FIT} + SS_{PURE}$$

with $$SS_{TOTAL} = \sum_{i=1}^{n} W(i) \cdot \Psi_E^2(i) \;,\; SS_{FIT} = \sum_{i=1}^{n} W(i) \cdot \overline{\Psi}_E^2(i) \;\text{ and }\; SS_{PURE} = S^2 \cdot (n-p) \tag{22}$$

The SS_{TOTAL} is the total variation of the data Ψ about zero, the SS_{FIT} is the variation about zero due to the fitted function, and SS_{PURE} is the variation about the fitted function. As the beam profile is estimated from the deviation of the data from the modulation function (ie., apart from the statistical fluctuation, the fit is always perfect), the SS_{FIT} is estimated from the smoothed version of the data, $\overline{\Psi}$.

An assessment of the linearity of the problem about the solution point can be obtained from a comparison of the uncertainty estimates derived by the two methods, viz. the contour and the linearised model. Further, for a linear system, the cost contour given by equation 18 should be symmetrically placed about the solution point.

Uncertainty estimates using these two methods are shown in figure 18 for the two parameter (source depth and CPA range) problem. The marked box indicates the uncertainty bounds derived from equation 21. Both tests of linearity are seen to fail. The sizes of the estimated bounds are in strong disagreement, indicating a breakdown of at least one of the assumptions given above. The appropriate method of determining the uncertainties in the parameters is to use equation 18, however a determination of the contour, or surface, is required.

If the total cost function, being the geometric mean of the several separate cost functions, is used, the above analysis is incorrect as the cost function is no longer a pure sum of squares. As this will be the function to be minimised in the algorithm described in this report, the independent linearised bounds can be used as quickly evaluated guides to the uncertainty levels, although strictly the confidence level will not be known. The overall uncertainty in the variables will typically be dominated by the uncertainties in the fixed quantities, in particular the source speed, rather than the uncertainty due to the least squares optimisation, and some sort of variational analysis, such as described above, would then be more appropriate in defining confidence levels.

5. Conclusions

This report has considered how to utilise the Lloyd's mirror interference pattern often associated with measured narrowband signals; in this case those signals obtained from a single omni-directional sensor. Rather than seeing the interference as a nuisance, the fringe positions can be used to estimate the source-receiver relative position; information that would otherwise be unavailable from a single sensor. The present study has outlined a standard least-squares optimisation approach to extracting this information from a set of narrowband line data. Whilst the analysis has been based on an iso-speed medium, the structure of the algorithm is equally suitable for any range independent propagation loss model.

We propose that the narrowband received signal strengths be separated into two components - an estimate of the intrinsic signal strength as would be measured in the absence of interference, and the interference modulation function. The interference modulation is directly determined by the source-receiver geometry, and thus this allows multiple line data sets to be considered simultaneously, and used in a global least squares search for the underlying geometry. Such a separation is properly valid when the source sound beam patterns have only an azimuthal dependence, and the boundary reflection can be treated as glancing angle and frequency independent. The least squares cost function is derived from the modelled and estimated modulation functions. This modulation function is estimated by passing the measured signal strength data through a running average filter. This should be adequate as the interference fringes are roughly periodic, at least for those data near to the time of CPA. For those narrowband lines where the interference modulation is clearly not periodic (when the signal frequency allows only one or two minima either side of the

time of CPA) this filtering is inappropriate, and the method cannot be used on these data.

To make the problem tractable, the source is assumed to move at a constant velocity and depth. This reduces the parameterised trajectory description to four variables - the source speed and depth, the range from the receiver at closest point of approach and the time of closest approach. We assume that the speed and time of CPA are known, along with the fixed receiver depth. Then the optimisation is required to determine the source depth and CPA range as well as a boundary reflection coefficient. An unique solution cannot be determined for the iso-speed medium in that the source speed, the source and receiver depths and the CPA range are coupled. Thus, the accuracy of any estimated solution point will be strongly dependent on the least well determined of the "known" quantities. This will typically be the source speed, which can be extracted from a Doppler analysis of the frequency dependence of the same narrowband line data.

We propose that the optimisation is based on a discretisation of the source depth and CPA range parameter space. Ideally, the reflection coefficient is uncoupled from these parameters, although signal noise and elevation dependencies will weaken this. Data weighting, which effectively biases towards the CPA time where the data is most clearly affect by the interference, improves this separation. The grid spacing must be based on the anticipated variation of the propagation loss with the source depth and CPA range, and the iso-speed model allows an analytical estimation of this. With a suitably small grid cell size, no further useful information concerning the depth and CPA range will be obtained. The structure of the cost function on such a grid is found to be complex and no single minimum can be expected. Rather, a series of valleys, each representing an approximately constant phase relationship between the direct and reflected waves, will be present. Two problems are posed by this. Firstly, the appropriate bounds on the parameter space must be ascertained and, secondly, the manner of the optimisation needs to be considered. The parameter space bounds can realistically only be decided from other information, such as the estimated CPA range produce in a Doppler analysis, or from practical limits on the source depth.

The structure of the cost function is considerably simplified by including multiple narrowband line data sets, covering a wide frequency range. The total cost function is taken as a geometrical mean of the individual line data cost functions. In a frequency independent environment such as we have here, the size and positions of the structures in the cost function will scale with frequency (ie. they are strictly phase dependent), and therefore any combined cost function will tend to accentuate the true solution point minimum whilst averaging out other variations in the cost function surface. This will help in obtaining the proper solution, however the problem of multiple minima is not removed. Two methods are suggested. The first is to apply a simulated annealing algorithm to the optimisation. Such algorithms are particularly suited to detecting global minima amongst multiple local minima. The second approach is to iteratively search the parameter space looking for potential solution points and testing these against the collection of the line data. We propose that this is

done using the total cost function, and with a coarse grid cell size. The higher frequency data will improve the sensitivity to the parameter values, although at the expense of a smaller grid cell size, and potentially a longer computation time. Indeed, if the bounds on the parameters is not large, it may be appropriate to evaluate the total cost function over the full grid and directly isolate the solution point. Once a suitable region is isolated, a direct search optimisation algorithm can be employed to provide the appropriate solution point. The important point is that the weighted sum of squares cost function based on the interference modulation function allows a two parameter search using data from several narrowband lines in a manner only dependent on the underlying source-receiver geometry.

The simulated annealing algorithm lends itself to an automatic optimisation. Being essentially a random sampling of the parameter space, it is not an efficient technique however it is robust. We find that such an algorithm will detect the correct solution point from a complex cost function surface, although owing to the need to evaluate many cost function values, it can be slow. This is the most straightforward of the two methods, and by choice the preferred option. Being a probabilistic solution, the solution point can never be guaranteed to be the global minimum, and the results from the annealing algorithm always should be verified by evaluation of the modulation functions for each of the narrowband lines. Any significant mismatch would indicate a poor solution.

In the end, the decision on how to proceed will be determined by the quality of the data, the a priori knowledge of the system and the speed of computation.

6. References

1) P.R. Lewis, *The Effect of Ray Curvature on Lloyd's Mirror Fringe Estimates and Source Localisation*, DSTO Technical Report DSTO-TR-0064, 1994.

2) *SIMDOP16, A programme to produce simulated data time series*, D.R.A. McMahon, unpublished.

3) *AMADEUS, Users' Guide V1.7*, 1994, D.R.A. McMahon & G.K. Schwarz, DSTO General Document DSTO-GD-0073.

4) *CASCADE, A Computer Aided Sonar Classification and Data Extraction System*, Ebor Computing, unpublished.

5) MATLAB V4.2c, 1995, The Mathworks Co.

6) The 1985 Baseline Passive RAYMODE propagation Loss Prediction programme (V8.0), unpublished.

Appendix A

Parameter estimation using a Simulated Annealing algorithm

For cost function surfaces with a complex structure of local minima and valleys, it is non-trivial to produce an automated optimisation algorithm which is capable of locating the global minimum on the surface. Standard searching algorithms provide a method of descending a local valley, generally utilising gradient information, and efficiently locating the local minimum point, and are not suited to such a problem. The simulated annealing algorithm provides a way of sampling the parameter space in such a manner that it will converge to the global minimum with a high probability. The method requires only cost function value evaluations to be made, and as such is well suited to the optimisation of discrete functions.

The algorithm is derived by analogy with the adiabatic cooling of a thermodynamic system, in which the global minimum energy state is achieved. Adiabatic cooling requires that the temperature is reduced sufficiently slowly that the system remains in thermal equilibrium. At any temperature, the particle energies are distributed according to a Boltzmann distribution and there is always some probability that a particle of any particular energy will exist, with this probability diminishing with the reduction in temperature. The analogy to a function minimisation proceeds as follows:

- The system energy $\Leftrightarrow$ The cost function
- The configuration of the particles $\Leftrightarrow$ The set of possible parameter combinations
- The temperature $\Leftrightarrow$ The searching control parameter

The basic structure of the algorithm is that at each temperature, a random sequence of parameter configurations is generated. A particular configuration is accepted if it either produces a smaller than current cost function value, or with a Boltzmann distributed probability determined by the temperature. In this way a sampling of the parameter space is performed, and after some number of configuration steps, the sampled cost function should converge such that the average value is unchanging. The best point found during this sampling then serves as an initial point for the next cycle, which occurs at a lowered temperature. The best point should converge to the optimal point with the reduction in temperature. Thus, in the early stages, at a "high" temperature, a random sampling of the space is done. As the temperature is reduced, the best point will settle into one of the many valleys, although it is always possible for this point to jump to a new valley, and thus allow the exploration of a new parameter region. The probability of doing this, however, diminishes with the temperature reduction.

The components of the algorithm which need to be specified are the rules for the selection of a parameter configuration, the number of configurations to be tested, the method of reducing the temperature at each cycle and the termination criteria. Because the algorithm only uses the cost function values, and samples the parameter space in a

pseudo–random manner, it will generally be more wasteful of function evaluations than one guided by gradient values, however this also makes it better suited to automated optimisation. The details of the algorithm used in the present application are given below.

As observed on §3.1, the effect of the reflection coefficient is approximately decoupled from that due to the source depth and range at CPA. Therefore, only a two parameter search is considered, and the cost function is discretised on a grid constructed by the methods of §2.1. An initial point on the grid is selected randomly.

The temperature dependence at cycle (i+1) is given by

$$T_{i+1} = \alpha T_i \quad \text{with} \quad 0 < \alpha < 1 \tag{A1}$$

The value of α will determine the rate at which the system is cooled. The cooling rate is important since if it is too slow, the number of cycles required for proper convergence, and hence the number of function evaluations, will become excessive. Conversely, if too fast, the system will never achieve an equilibrium state and the solution point, if any, will not be the global minimum. The appropriate rate of cooling will depend on the scheme used to select the parameter configurations. The cooling rate can be larger if the potential configurations available from the current configuration (the "reach") cover most of the valid parameter space, because at each step in a cycle the probability of moving out of the current region to a, perhaps, more favourable region is higher.

It is desirable to bias the reach toward the current point, since then more of the sampling is done about what is currently the best estimate of the global minimum. Therefore, within a cycle, the configuration selection is

$$x_{i+1} = x_i + \Delta x \cdot \text{sign}\left(R[-1,1]\right) \cdot R[0,1]^N \quad \text{with} \quad \Delta x = \beta \cdot (x_{max} - x_{min}) \tag{A2}$$

where R[a,b] is a uniformly distributed random number in the interval [a,b] and x_i is the parameter value at the i^{th} step of the cycle. The Δx is the maximum allowable step. When there are multiple parameters, each parameter is sequentially modified. If the new parameter value exceeds the bounds of the parameter interval, the value is reflected back into the interval as

$$x_{i+1} \rightarrow \begin{cases} 2x_{max} - x_{i+1} & x_{i+1} \geq x_{max} \\ 2x_{min} - x_{i+1} & x_{i+1} \leq x_{min} \end{cases} \tag{A3}$$

The non-uniform random distribution of the step sizes allows coverage of the entire range specified by Δx, but favours configurations near to the current position. On a discrete grid, the value of (x_i+1) is rounded to match the nearest grid position. Care needs to be taken if the discrete grid is small, as the power N in equation A2, if too

large, will cause most of the new parameter configurations to match the current configuration.

A parameter configuration is accepted if either the resultant cost function is smaller than the current cost function, or if, at cycle i, the change in the cost functions ΔC satisfies

$$R[0,1] < \exp\left(-\frac{\Delta C}{T_i}\right) \quad \text{for} \quad \Delta C > 0 \qquad \textbf{(A4)}$$

The initial temperature T_0 is selected to be larger than the largest expected cost function deviation.

A cycle is terminated when either the number of new configurations exceeds a preset level, N_S, or the number of attempts at finding a new configuration exceeds a preset level, N_A. The former condition carries the assumption that after N_S successful new configurations, the system has settled to an equilibrium point. The latter condition ensures that each cycle will terminate even when a new configuration can not be found. Appropriate values for N_S and N_A will depend on the rate at which the system is cooled. At the termination of each cycle the configuration producing the lowest cost function is chosen as the initial point for the next cycle of the process, continuing at a reduced temperature.

The annealing process is terminated when either the number of successful new configurations for the previous cycle is zero, the same best configuration is repeatedly found over a number of cycles, N_R, or when the number of temperature reductions exceeds a preset level, N_T. The first condition signifies a true convergence to a solution point; similarly with the second, although this prevents any oscillation about the solution point over several cycles. Again, the latter condition is a fail-safe termination condition.

The values chosen for the present application are $N_S = 15$, $N_A = 60$, $N_R = 10$ and $N_T = 40$. The cooling factor is $\alpha = 0.65$, the step size scale factor is $\beta = 0.5$, and the step non-linear random number distribution is generated with a power of $N = 2$. Once suitable choices for these parameter values have been made, the annealing optimisation is particularly straightforward. The difficulty is in selecting values that will ensure an adequate sampling of the parameter space, whilst providing good convergence within a reasonable amount of time.

Examples of the result from a two parameter search for the examples of §3.1 are shown in figures 14 and 15. Figure 14 shows the sampled cost function during the search, and how the algorithm samples the entire parameter space, but concentrates on the region near to the estimated solution point. The variation in the cost function at the best estimate of the solution for each cycle, and examples of the sampling within each cycle are shown in figure 15.

Appendix B

The LINAL analysis interface

To facilitate the analysis of narrowband data, a prototype analysis programme has been developed. This is a menu driven interface written using the MATLAB [5] data analysis package running under UNIX. It provides all of the analysis features discussed in the body of the report, and was used in analysing the simulation data therein. Most of the functions are written as MATLAB shell scripts, and thus are easily modified. To improve the execution speed, the cost function evaluation routine is a compiled C module.

COMMAND STATUS			
SOUNDSPEED PROFILE FILENAME	LINE DATA FILENAME	BACKGROUND DATA FILENAME	WORKSPACE FILENAME
LOSS DATA FILENAME			
FILE OPTIONS	CALCULATION OPTIONS	DISPLAY OPTIONS	SOURCE PATH
GRID CONTROL	ANNEALING CONTROL	MINIMISATION CONTROL	
GRID SOLUTION	ANNEALING SOLUTION	MINIMISATION SOLUTION	

The menu display is shown in figure B1. The information is divided into the following sections:

- COMMAND STATUS — the status of the current command
- FILENAME — the names of the various active data files
- FILE OPTIONS — the file open, load and save options
- CALCULATION OPTIONS — the various data calculation options
- DISPLAY OPTIONS — the various data display and printing options
- SOURCE PATH — the description of the current source trajectory solution
- GRID CONTROL — the parameter grid control parameters
- ANNEALING CONTROL — the simulated annealing optimisation control parameters
- MINIMISATION CONTROL — the simplex least squares optimisation control parameters
- GRID SOLUTION — the current search parameter grid
- ANNEALING SOLUTION — the simulated annealing optimisation trajectory solution
- MINIMISATION SOLUTION — the simplex least squares optimisation trajectory solution

A description of the various options available in each section is given below.

B.1 Filename

Five files are used by the programme: the sound speed profile description, the narrowband line profile data file, a background noise spectrum data file, a workspace file and a loss data file. The files provide for

- the sound speed profile description, which is an ASCII text file containing a list of depth, sound speed pairs. Each record lists one pair of space separated values giving the depth (metres) and sound speed (metres/second). Blank lines and lines with a % (comment lines) as the first character are ignored. If only a single data pair is present, it is interpreted as the water column depth and the constant sound speed for this column.
- the line profile data, which is a CASCADE [4] formatted text file. This contains the narrowband line Doppler shifted frequency, signal strength and time values. It is produced using AMADEUS [3].
- the complete state of the current analysis environment to be saved to a MATLAB binary format workspace file. This allows standard configurations to be established, or for a continuation of an analysis session at a later date. The currently displayed figures are not saved.
- a background noise level frequency spectrum to allow background noise subtraction. The file is an ASCII text file giving the power level in dB/Hz. Each line contains one pair of space separated values giving the frequency (Hz) and background level (dB/Hz). Blank lines and lines with a % (comment lines) as the first character are ignored.
- the internally generated loss data to be saved to a MATLAB MAT binary file. This may be of use when the required loss data is computationally expensive to produce.

B.2 File Options

These options control the loading and saving of the various data files. The options available are to

- load the sound speed profile
- load the narrowband line data
- load a background spectrum
- load previously saved loss data
- load a previously saved workspace description
- save the currently evaluated loss data
- save the current workspace description
- exit the programme

Loading any of the sound speed, line data, background, workspace or loss data files will cause the current filename entry to be modified. If the workspace is altered from

that defined by the currently loaded file, the filename is marked with an asterisk to indicated this. When the line data file is loaded, the programme will prompt for the natural frequency of each of the narrowband lines, whilst indicating the estimate of this based on the doppler shifted frequency values.

B.3 Calculation Options

These options control the calculation of the various quantities, and the operation of the optimisation routines. The options available are to

- generate the data grid
- calculate the propagation loss data on the defined grid
- calculate the cost function on the defined grid
- determine an optimal solution using the simulated annealing algorithm
- determine the optimal solution using a simplex least squares minimisation algorithm
- set the data smoothing/filtering window sizes for each narrowband line
- select new grid limits from a currently displayed cost function surface
- set or modify the background levels at each of the line data frequencies

A menu button is used to

- set the cost function weighting mode

Several switches, one per line frequency, to

- select or unselect the various line data sets from the optimisation

The sequence for performing an analysis is to load the appropriate sound speed profile, narrowband line data and, possibly, a background noise spectrum. When the line data file is loaded, the pushbuttons, one per frequency, will be enabled. When pressed, these buttons include/exclude the associated data from the optimisation process.

Before any calculation can proceed, a data grid must be defined using the **Data Grid** option. The size of the grid is determined by the parameters in the **Grid Control** control panel. The size of the grid will in part be determined by the highest frequency selected, and increases as the square of this frequency. All calculations are based on the current grid. Changing the selected frequencies will issue a warning that the displayed grid, loss data and cost function data are no longer valid.

The **Loss Data** option allows the loss data to be generated for the current grid and the current frequency selection. Changing the frequency selection will clear the current loss data. The sound speed profile determines the manner of the propagation loss calculation. If the sound speed is constant, the analytic expressions are used, otherwise, a range independent propagation loss programme is utilised. The propagation loss is internally generated if an iso-speed profile is used, otherwise via an external programme.

The relevant function is *loss.m*. As currently setup, this calls a further function *raymode.m* which acts as an interface to an independent propagation programme RAYMODE [6]. This programme utilises the UNIX stdin and stdout I/O files to accept data and to return the results of any calculations. The UNIX pipe functionality is used within *raymode.m* to send a formatted input deck to RAYMODE and to read the formatted output. A UNIX Awk script is used to scan the programme output and extract the relevant propagation loss data. The details of this are hidden inside the *raymode.m* function. This function and the calling sequence within *loss.m* is specific to the actual propagation loss programme used. Any programme that uses the stdin and stdout for data I/O can be used, although the function to call it and extract the relevant data will need to be tailored to the programme. The calling sequence inside *loss.m* will also need to be altered.

The total cost function surface can be evaluated for the current frequency selection and the current grid with the **Gridded Cost Function** option. The loss data must be defined before the cost function is evaluated. Changing the frequency selection will clear the current cost function data.

The simulated annealing solution, using the parameter values currently defined in the **Annealing Control** panel, is produced using the **Annealed Solution** option. Only the source depth and the range at CPA are determined. No uncertainty estimates are produced All trajectory and receiver parameters are obtained from those currently defined in the **Source Path** control panel.
The least squares optimisation, using the parameters currently defined in the **Minimisation Control** panel, is produced using the **Fit Solution** option. The source depth, range at CPA and the reflection coefficient are determined, as specified. All trajectory and receiver parameters are obtained from those currently defined in the **Source Path** control panel. A simplex algorithm, which uses only the function values at the simplex vertices, is used. No constraints are imposed on the parameter values. The MATLAB *fmins.m* function implements this function minimisation routine.

The definition of the cost function requires an estimate of the unmodulated line profiles. These are determined as discussed in §2.3, and require an estimate of the smoothing filter window. The size of this will depend on the frequency of the narrowband line data. The estimates are currently obtained from user defined values. The **Smoothing Window** option is used for this. On selection, each line data set will be displayed in sequence. The positions of the interference minima must be marked in using the cursor (left button to select, middle button to remove, right button to end). A window size is then determined from an average of the marked minima separations about the time of CPA. It is therefore important that, where possible, adjacent minima are marked. For reference, the current value of the time of CPA defined in the **Source Path** control panel will be shown. The estimated window widths at each frequency are listed.

The **Select on Grid** option is provided to simplify the selection of a region of the parameter space of interest, and can be selected whenever a cost function surface is

displayed. A sub-region of the current parameter space (the source depth and the CPA range) is selected using the cursor. The appropriate limits are then transferred to the **Grid Control** panel. To operate the cursor, firstly a figure displaying a cost function surface is selected (left button), followed by the sub-region definition (left button). A rubberband box shows the selected region.

The background noise levels can be optionally included via the **Load NB Line Data** option of the **File Option** panel. If no file is loaded, a zero level background is assumed. Alternatively, the **Set Background Levels** option can be used. This will modify the current levels, be they externally defined, or the default levels. The values are in dB/Hz, and are specified at the defined line data frequency values.

The cost function is evaluated from the set of line data signal levels. The contribution of each datum can be optionally weighted. The **No Weighting/Smoothing** menu button determines the current state. The data weighting, if applied, follows the definition of §2.3. By preference, the data should be weighted.

Switches control the selection of the data to be included in any optimisation. Changing the data selection will render any previously calculated propagation loss data, parameter grid and cost function values invalid.

B.4 Display Options

A number of display and hard copy options are provided. These are collected in the **Display Options** panel, and comprise options to

- plot the current sound speed profile
- plot all the currently loaded narrowband line data
- plot all the currently loaded line data together with the current fit
- plot the fit residual based on the current line data and fit
- plot the smoothed current line data
- plot the ratio of the current line data to the current smoothed line data
- plot the current propagation loss data
- plot the current cost function generated with the **Gridded Cost Function** option
- plot the current cost function resulting from the current simulated annealing optimisation
- print the figure as selected
- print the current set of figures
- clear the figure as selected
- clear the current set of figures

The number of plots shown for any of the plotting options depends on the data to be displayed. The current set of figures is consists of the complete set of plots created by the most recent plotting command. This set can be printed, with one plot per page, or deleted. In this latter case, the current set of figures reverts to the previously most

recently defined set. As well, an individual plot can be printed or deleted. When chosen, a prompt for the figure to be printed or deleted is given, with the selection being made with the cursor.

The **Sound Speed Profile** plot consists of a single figure showing the current sound speed profile.

The **NB Line Data** plot consists of multiple figures, each showing six line data sets. All the currently defined data, irrespective of the status of the current data selection, are displayed. Similarly, the **NB Line Data & Fit** plot consists of multiple figures, each with six line data sets, together with the estimated profiles based on the current trajectory parameters. The loss data necessary for these profiles are calculated when this option is chosen, with the manner of calculation based on the current sound speed profile. The data in both cases are plotted in absolute units (ie. not dB).

The **NB Fit Residual** plot consists of multiple figures, each showing six line data sets. Here, the difference between the line data and the calculated profiles is shown. As above, the loss data, using the current trajectory parameters, are calculated when this option is chosen. The data are plotted in dB.

The **NB Smoothed Data** plot again consists of multiple figures, with six line data sets shown per plot. In this case the data before and after being passed through the smoothing filter are displayed. Similarly, the ratio of the line data to the smoothed version of the same data is shown with the **NB Data/Smoothed Data** option. These latter plots are in linear units, and if the data smoothing is adequate, should show as an oscillatory function of roughly constant amplitude. The size of the oscillations depends on the reflection coefficient, and as a guide to a suitable value, the lower and upper bounds of the oscillation, evaluated for an iso-speed profile (C_S = 1500 m/s) and with the reflection coefficients given in the **Source Path** panel, are plotted.

If the current propagation loss data, calculated using the **Loss Data** option in the **Calculation Options** panel, exists, it is plotted using the **Loss Data** option. One figure is shown for each active line data set. The loss data are plotted as a function of the source depth and the horizontal range from the source for a fixed receiver depth and source frequency.

The **Gridded Cost Function** option plots the total cost function calculated on the parameter grid using the **Gridded Cost Function** option in the **Calculation Options** panel. Only the currently active line data sets are used in the cost function evaluation. A single figure is produced. If a simulated annealing solution has been obtained, a by-product is the total cost function evaluated at the sampled parameter points. This can be used to show how the parameter space has been covered, or to define a smaller region of interest. The **Annealed Cost Function** option plots this function, if it exists. A single figure is produced. The cost function for both these options is plotted as a function of the source depth and the horizontal range at CPA.

B.5 Source Path

The current source straight line trajectory is specified using this panel, and all calculations are based on the current values of the parameters. These parameters are the

- horizontal CPA range (metres)
- slant CPA range (metres)
- time of CPA (seconds)
- source speed (metres/second)
- source depth (metres)
- receiver depth (metres)
- surface reflection coefficient
- bottom reflection coefficient
- smoothing factor

The quantities are self-evident. The CPA range can be entered as either the horizontal or the slant range. The associated value will be calculated from the current range and depth parameter values. The reflection coefficients are plane wave frequency and angle independent values. A reflection coefficient of zero will disable reflection from the associated surface.

The current values of these quantities are used in producing the modelled line profiles (ie. the loss data), in the determination of the parameter grid size, for defining the initial parameter values for the simulated annealing minimisation, and for the constant parameter values in the simplex least squares minimisation.

The values for the CPA range and the source depth can be read from the current cursor position on a cost function plot using the **Cursor Selection** button. Firstly, a figure displaying a cost function surface is selected with the cursor (left button). The cursor is then position on the surface and a point selected (left button). This point will be indicated with a cross hair. The values are entered in the **Source Path** panel. This allows primarily an estimate of the position of a local minimum to be read and the resultant match to the data to be tested. This can be used to assess the quality of the local minimum of the cost function as the best solution.

B.6 Grid Control

All calculations are based on a discrete parameter grid. This panel provides the control parameters for the grid determination. Three discrete sets are calculated, for the source depth and the horizontal range at CPA, and for the horizontal ranges associated with the propagation loss calculations. The parameters are the

- lower and upper limits on the horizontal CPA range (metres)
- lower and upper limits on the source depth (metres)
- step size scale factor for the range step in the loss calculations
- step size scale factor for the horizontal CPA range
- step size scale factor for the source depth

As well, three switches are provided to restrict the step sizes to

- a constant loss range step
- a constant CPA range step
- a constant source depth step

The lower and upper limits on the CPA range and the source depth define the region of parameter space of interest. The range limits for the propagation loss data are determined from the CPA range, the time of CPA and the time limits of the line data. The determination of the grid is defined in equations 7 and 9, which give the maximum step sizes consistent with the non-aliasing of the data within an iso-speed model.

The scale factors are needed for three reasons. To produce the estimates of the line profile data, the loss data is linearly interpolated at the ranges defined by the times and the current path parameter values. The quality of this interpolation will improve as the step size is reduced. Secondly, the necessary step sizes are expected to be smaller when a non-constant sound speed profile is used (eg. as shown by the lines of constant phase on a lofargram) [1]. In this case, it may be necessary to adjust the step size empirically in order that aliasing of the loss data does not occur. Lastly, there may be a requirement for a detailed exploration of part of the cost function surface.

The step sizes can be held constant at the smallest calculated values. The constant step switches select this option. In particular, depending on the programme being used the propagation loss data may need to be evaluated at equidistant intervals; thus the need for this functionality.

The current grid size is displayed in the **Grid Solution** panel. This is updated using the current parameters in the **Grid Control** panel along with the maximum active line frequency. The size of the grid and the minimum and maximum step sizes for each relevant parameter are displayed.

B.7 Annealing Control

This panel maintains the control values for the simulated annealing minimisation. The parameters are described in appendix A. The inputs are the

- maximum number of iterations per variable at each cycle (N_A)
- maximum number of successful configurations found per variable at each cycle (N_S)
- maximum number of cycles in the search (N_T)
- cooling factor (α)
- step scale factor (β)
- step size power (N)

Two switches are provided to

- list the information on the search as is proceeds
- plot the evolution of the search

The parameters correspond to those described in appendix A, as indicated by the quantities in the parentheses.

The minimisation information listed when the **List Fit Data** option is selected includes the

- iteration number
- current temperature
- current CPA range and source depth
- number of successful steps in the current cycle
- number of cost function evaluations made

At the end of the search, the information includes the

- final temperature
- final CPA range and source depth
- number of cost function evaluations made
- % hit rate (As the cost function is evaluated, it is saved. The number of cost function values that have been obtained from this saved list is expressed as a percentage of the total number of cost function evaluations made)
- % coverage of the grid
- % coverage of the CPA range space
- % coverage of the source depth space

Ideally, the % coverage in the CPA range and source depth should be close to 100%, whilst for a large grid the % coverage of the grid should be small. When the **Display Fit Data** option is selected, the information is shown on two plots. One shows the cost function for each successful configuration in the current step. The initial value is marked by a horizontal line. The average value of the cost function is overlaid on this. The other plot shows the variation in the best cost function value at each cycle, and thus how well the system in converging.

The solution point is displayed in the **Annealing Solution** panel. The two values thus produced can be transferred to the **Source Path** panel and used in the description of the current trajectory with the **Transfer Solution** option. No uncertainty estimates are produced. The simplex least squares method can be used to generate these by using the simulated annealing solution as the initial point to this routine.

B.8 Minimisation Control

The simplex least squares optimisation is controlled from this panel. Four parameters can be selectively varied. The initial values for these must be set. Three optimisation control values are required. The inputs are the

- horizontal CPA range (metres)
- source depth (metres)
- surface layer reflection coefficient
- bottom layer reflection coefficient
- maximum number of search iterations
- approximate fractional tolerance required for each parameter
- required absolute cost function tolerance

One switch is provided to

- list the information on the search as is proceeds

A switch is associated with each of the four parameters. This selects or unselects the associated parameter from being varied during the optimisation. The initial values for all four parameters are those given on this panel.

The optimisation control values default to a limit of 200 iterations, a 1% fractional tolerance in each parameter and an absolute tolerance on the cost function of 0.0001. The success of the parameter search will, in particular, depend on these latter two values. A successful search is achieved when both tolerance requirements have been met. The appropriate values in each case will depend on the structure and smoothness of the cost function surface; viz. the absolute magnitude of the cost function values, and its variation with the parameter values.

The minimisation information listed when the **List Fit Data** option is selected includes the diagnostic information from the simplex search, being primarily the current simplex value.

The solution point is displayed in the **Minimisation Solution** panel. Uncertainty estimates, based on the linearised least squares model outlined in §4, are produced and displayed with the solution point.

The four values thus produced can be transferred to the **Source Path** panel and used in the description of the current trajectory with the **Transfer Solution** option.

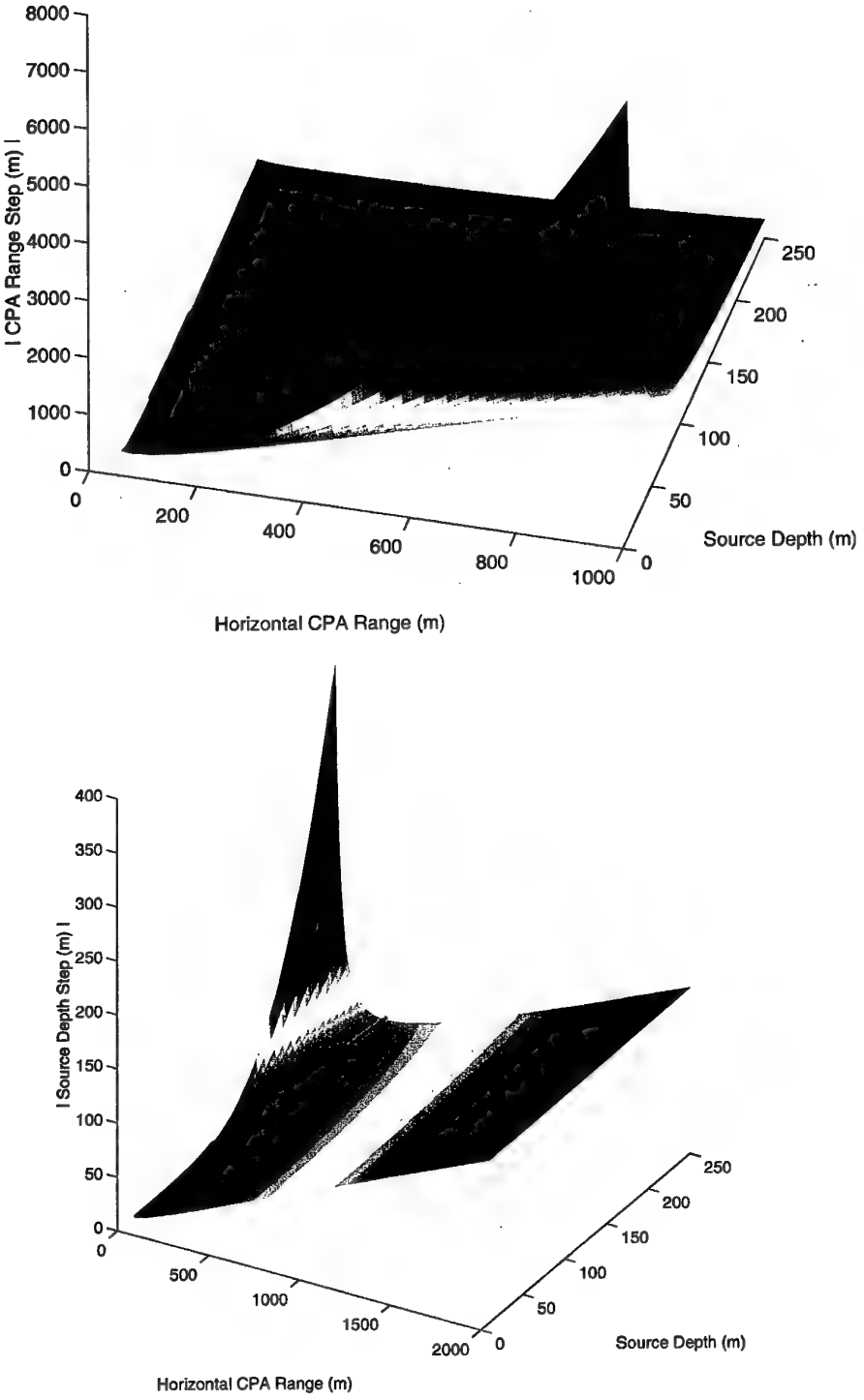

Figure 1 *Surfaces of the source depth and CPA range step sizes as a function of the source depth and CPA range. The values are obtained from equation 7, and are for a receiver depth of 100 m and a frequency of 150 Hz. The upper figure shows the absolute value of the step size in the CPA range, and the lower figure the absolute value of the step size in the source depth. The heavy curves on these surfaces mark the line of minimum value, as required by the data grid.*

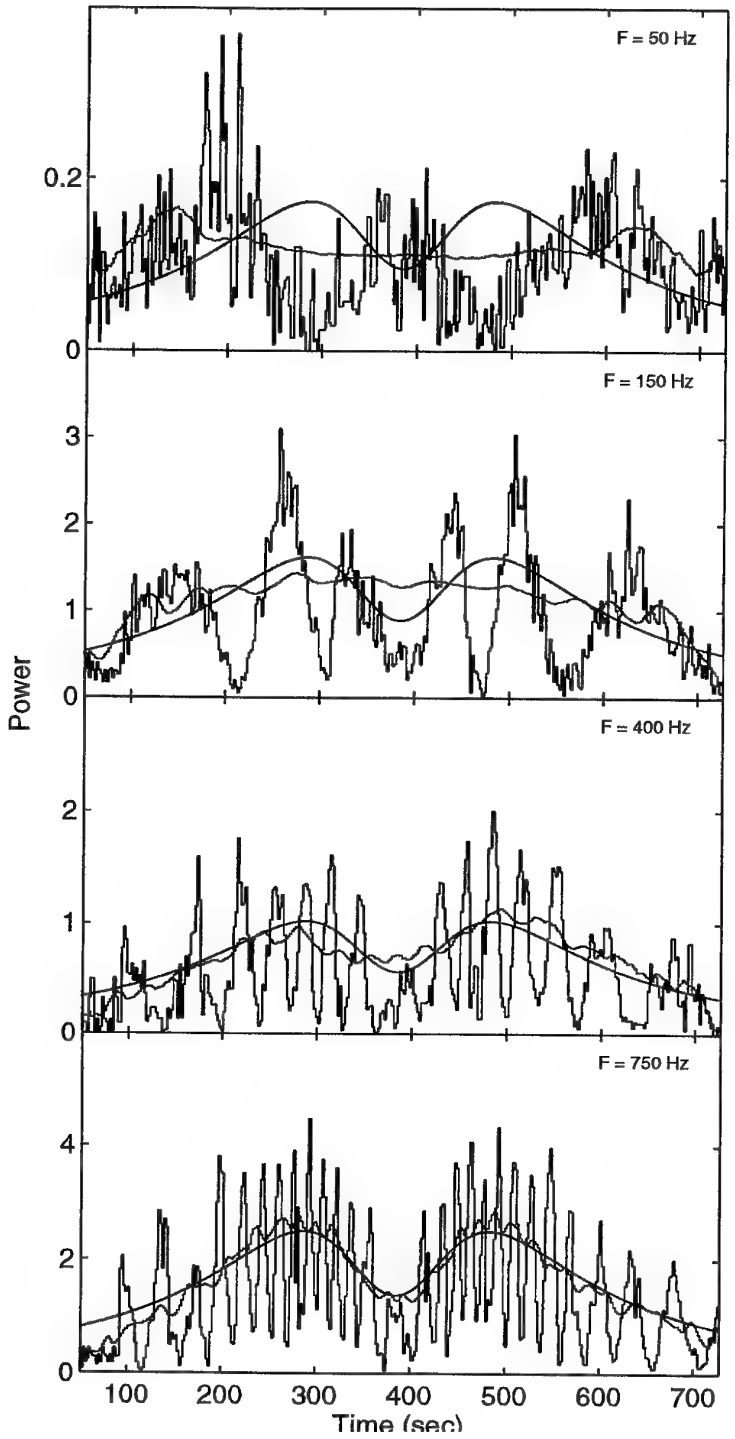

Figure 2a *Examples of the effect of smoothing the narrowband Lloyd's mirror interference pattern. The simulated data is for a dipole beam pattern. This figure shows the effect on the line profile, where the red and purple lines show the modelled and estimated beam patterns respectively. The 50 Hz data with only a single node pair is poorly reproduced, whilst the 150 Hz data with two node pairs is marginal. The higher frequency data are well reproduced.*

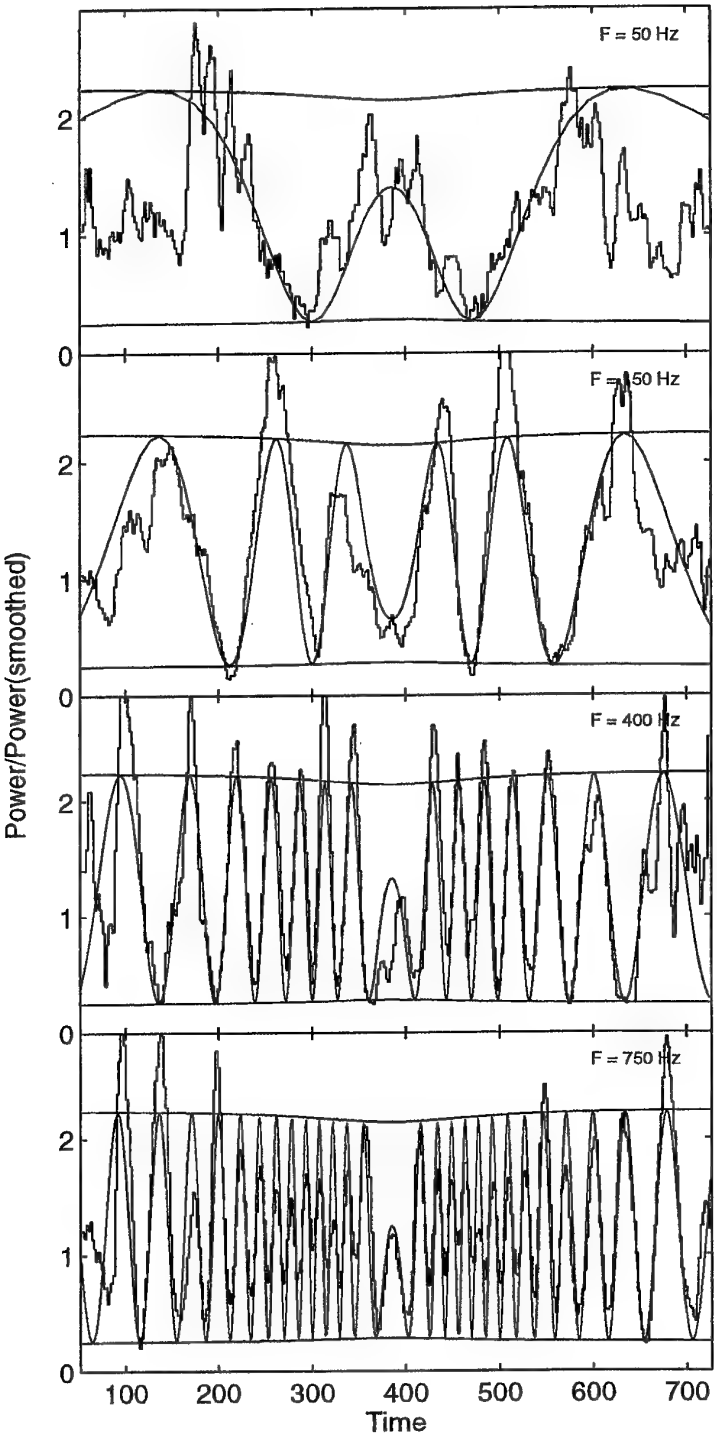

Figure 2b *Examples of the effect of smoothing the narrowband Lloyd's mirror interference pattern. This figure shows the modulation function deduced for the data in figure 2a. The purple line shows the modelled variation.*

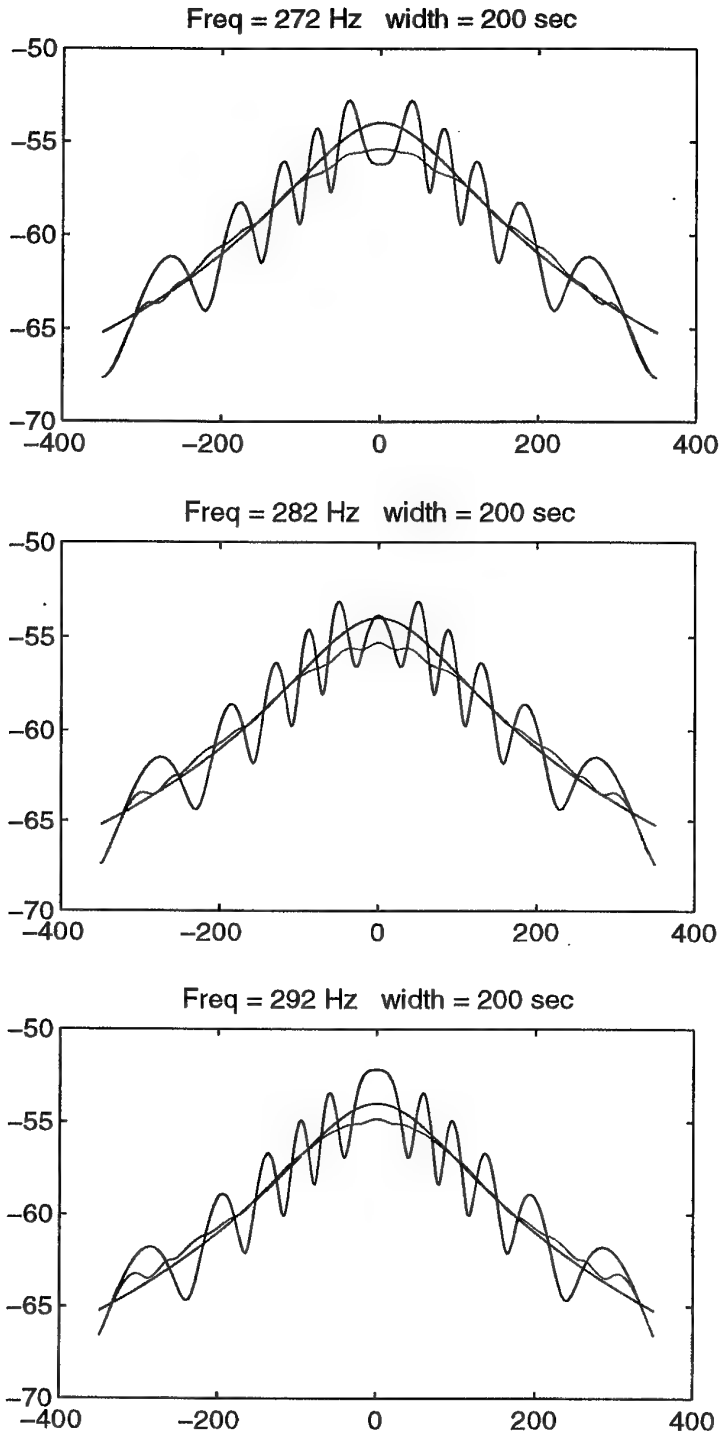

Figure 3a *The effect of data smoothing with a change in the phase value between the direct and reflected waves. The surface reflection coefficient is 0.25. The purple curve shows the modelled line profile. The upper plot corresponds to a phase difference at the CPA time of π, the middle to 0.5π and the lower to 0. The log of the data has been smoothed with a window four times the width of the estimated interference fringe width.*

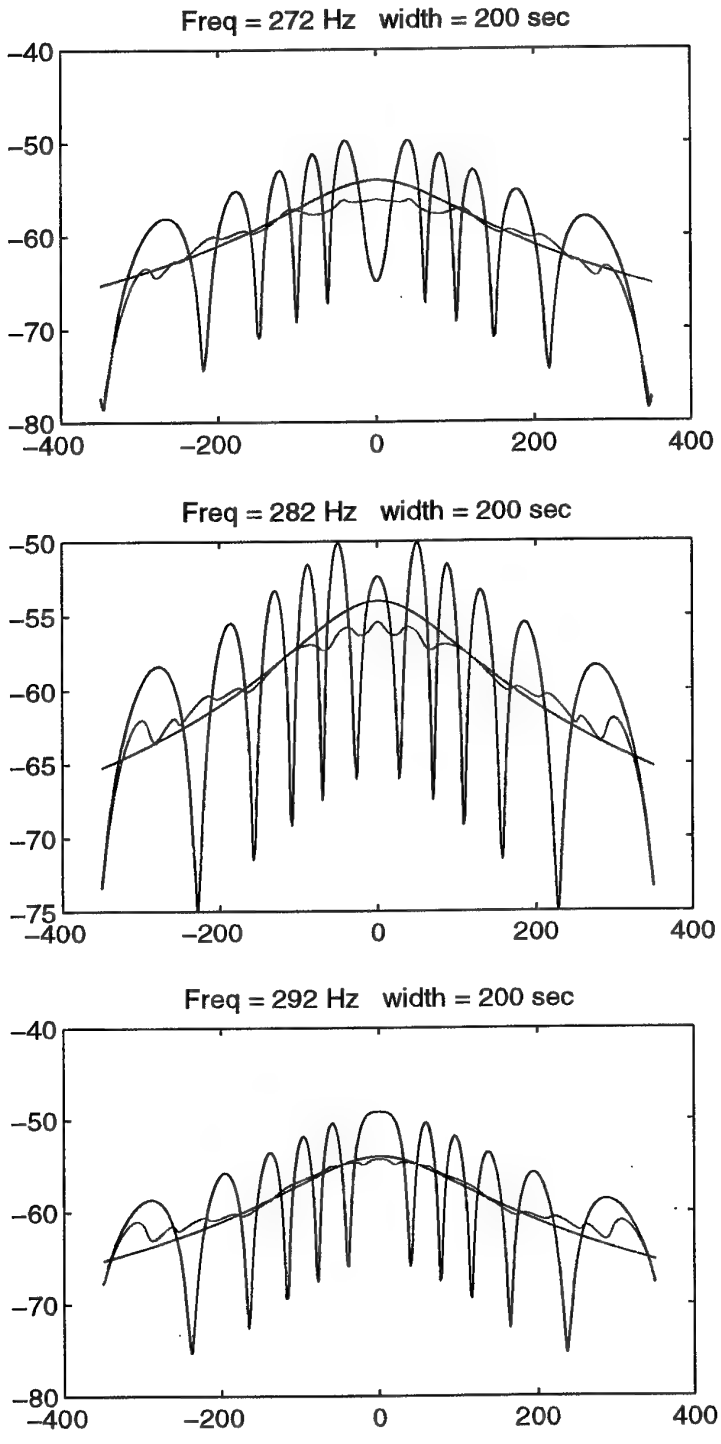

Figure 3b *The effect of data smoothing with a change in the phase value between the direct and reflected waves. The surface reflection coefficient is 0.8. The purple curve shows the modelled line profile. The upper plot corresponds to a phase difference at the CPA time of π, the middle to 0.5π and the lower to 0. The log of the data has been smoothed with a window four times the width of the estimated interference fringe width.*

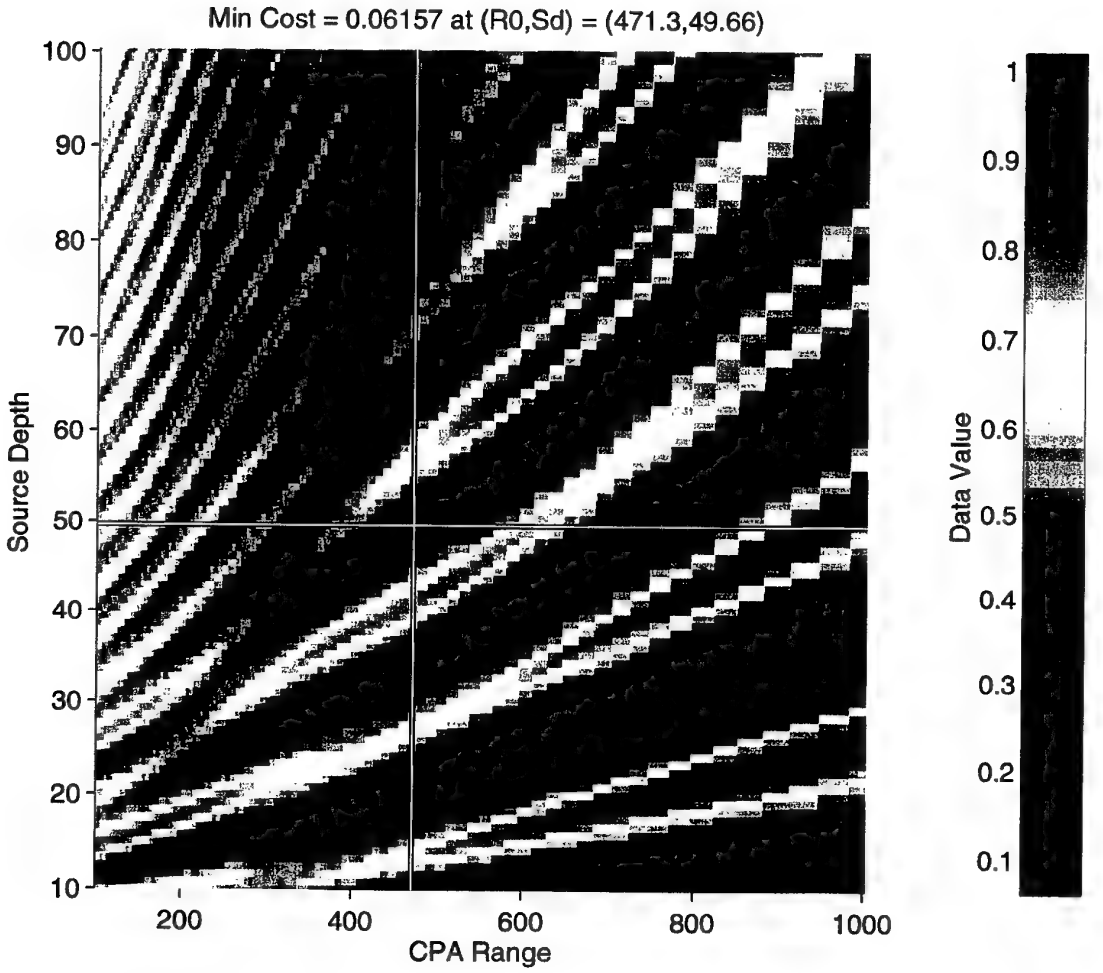

Figure 4 *The gridded least squares cost surface about the known solution point. The cost function is defined in equation 11. The modelled source has an isotropic beam pattern. A single narrowband line of frequency of 150 Hz was used and no data weighting has been included. The geometry is described in the text.*

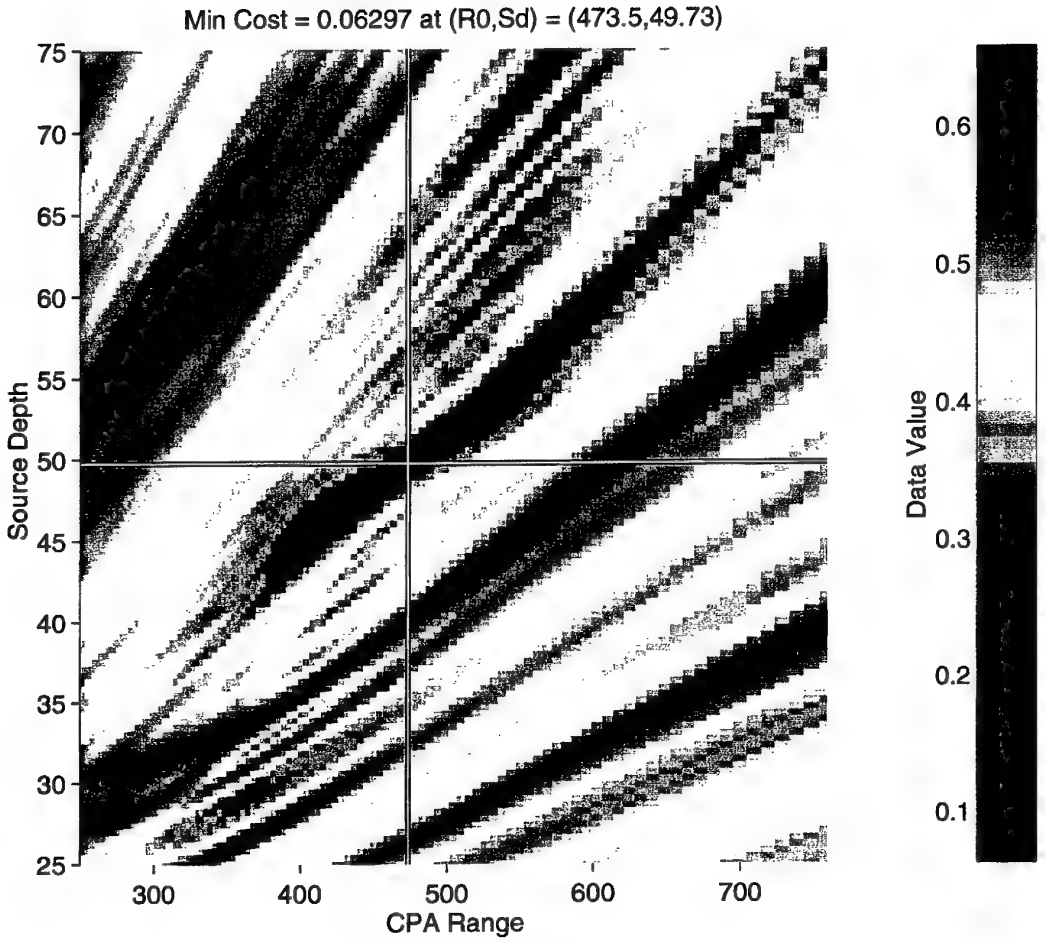

Figure 5 *The gridded least squares cost surface about the known solution point. The cost function is defined in equation 11. The modelled source has an isotropic beam pattern. Six narrowband lines of frequencies of 50, 150, 300, 400, 550 and 750 Hz were used. The cost function data has not been weighted. The geometry is the same as for figure 4, and is described in the text.*

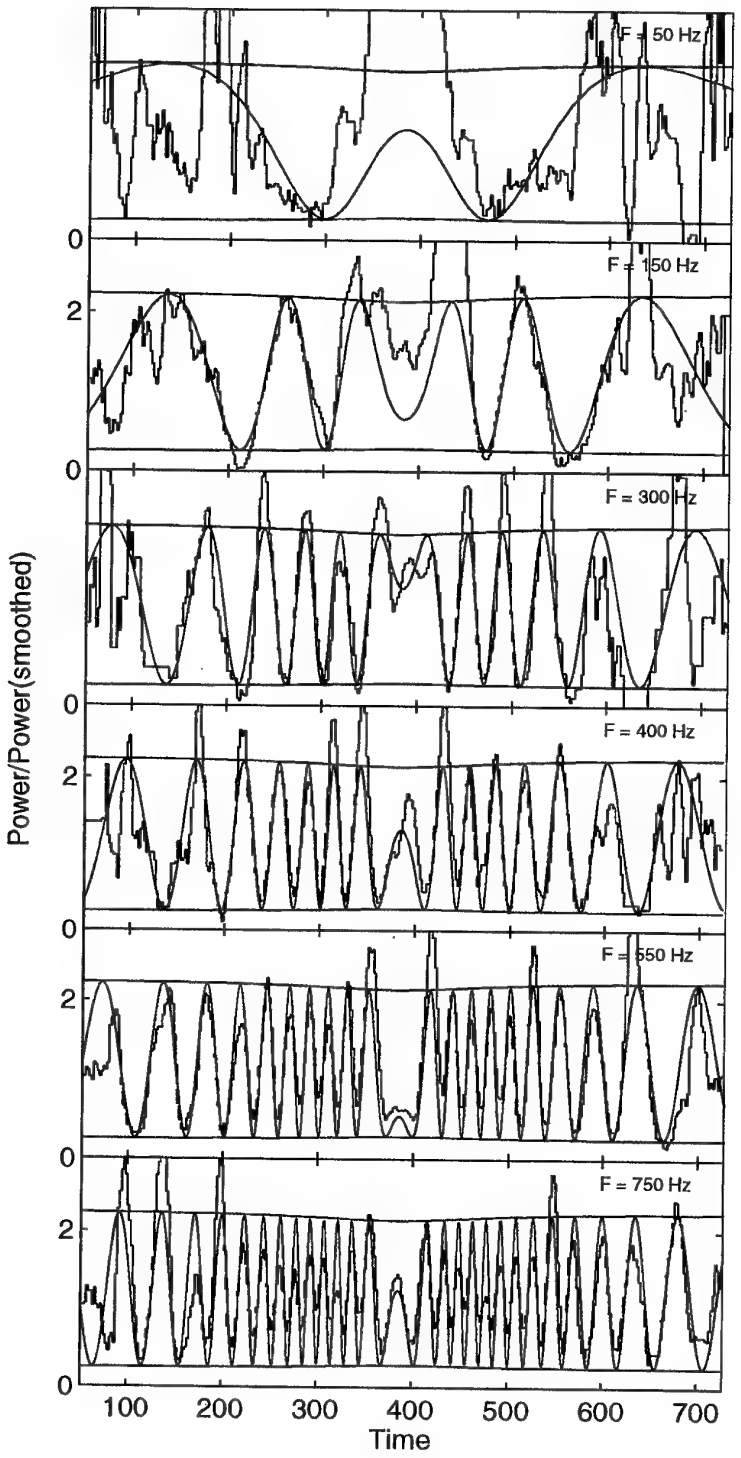

Figure 6a *The modulation functions for the six narrowband lines of figure 5. This figure is for the correct surface reflection coefficient of 0.5. The purple curve shows the modelled modulation function. The red bands define the modelled variation limits on the modulation function. The data for the 50 Hz line is in particular badly represented.*

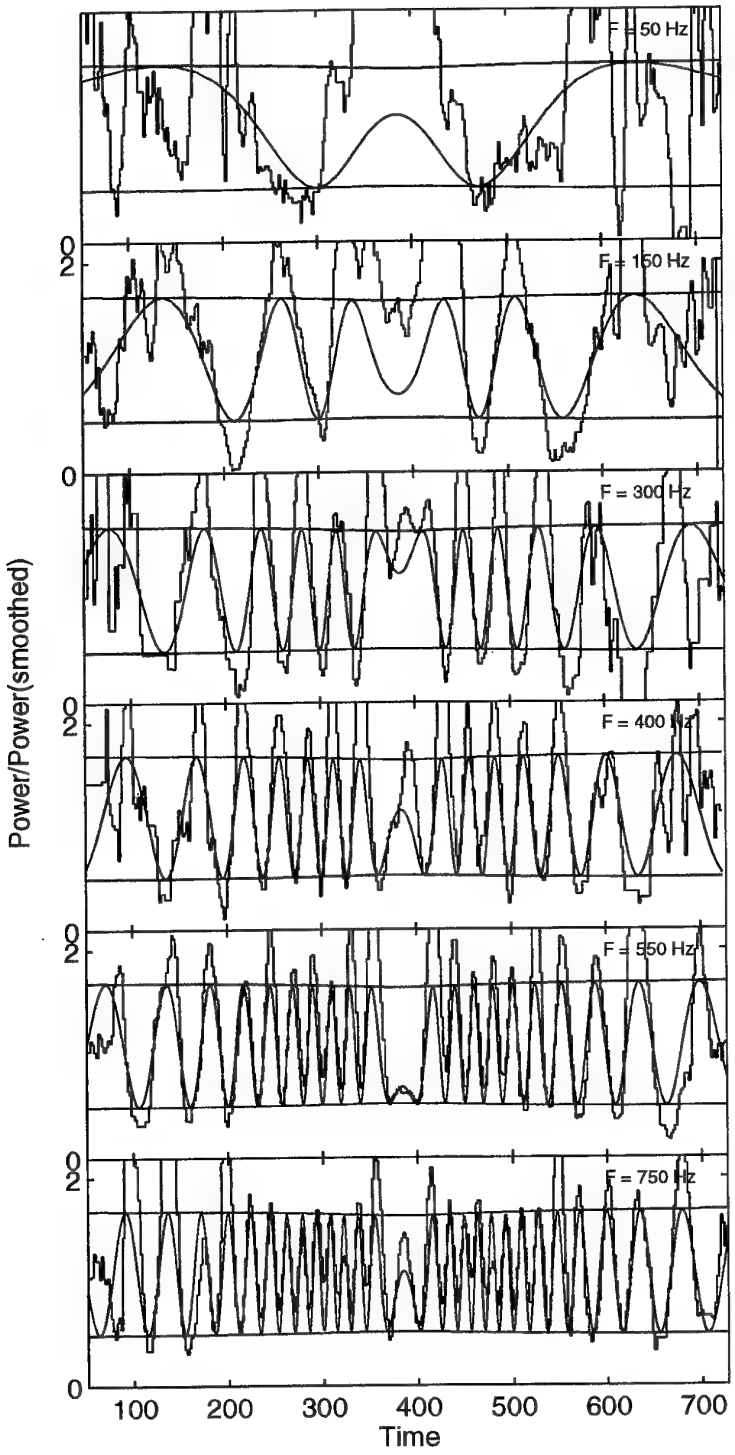

Figure 6b *The modulation functions for the six narrowband lines of figure 5. This figure is for a reduced reflection coefficient of 0.3. The purple curve shows the modelled modulation function. The red bands define the modelled variation limits on the modulation function. The data for the 50 Hz line is in particular badly represented.*

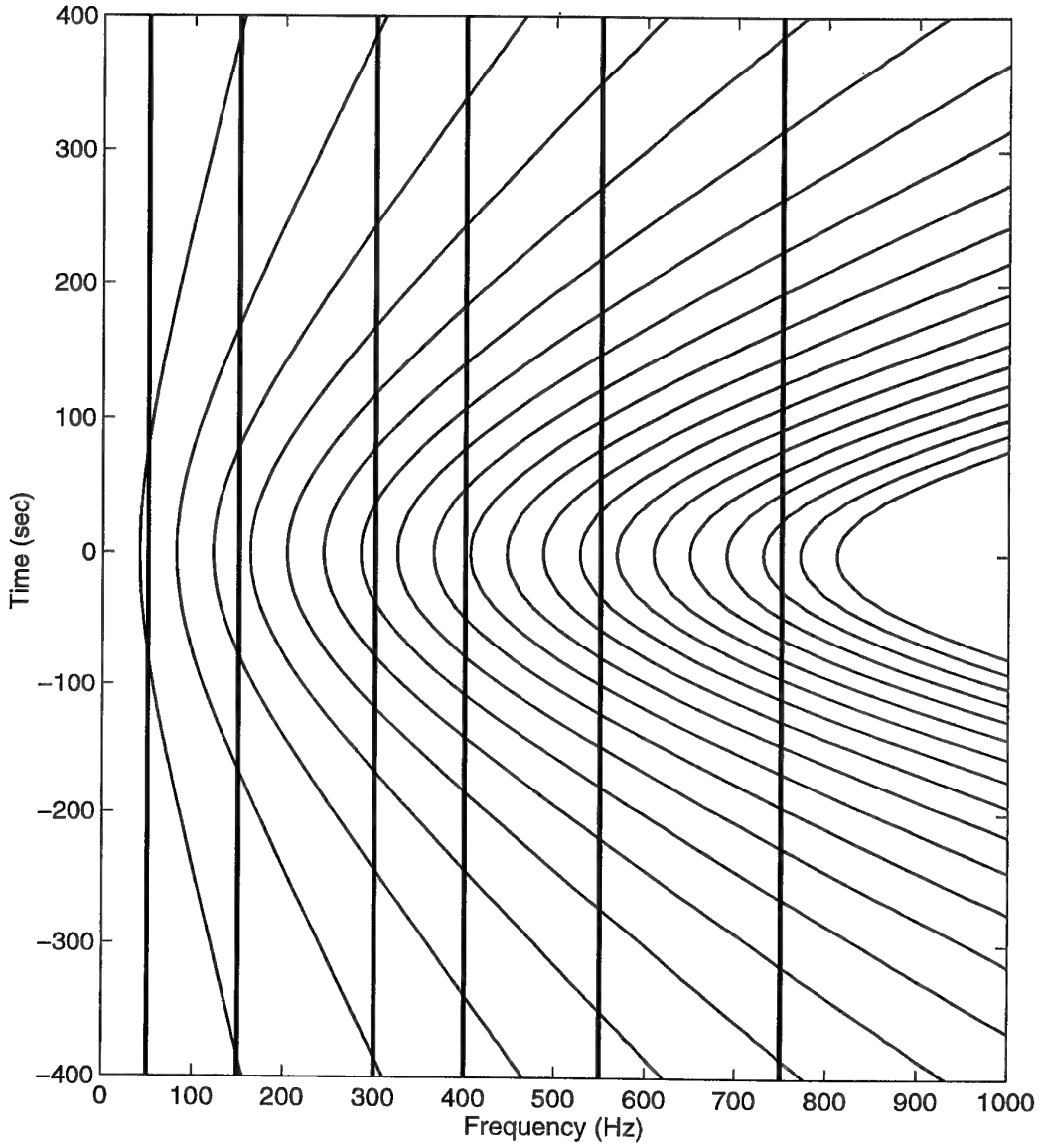

Figure 7 *The relationship between the narrowband line frequencies used with the present simulations and the broadband Lloyd's mirror interference pattern. The narrowband frequencies have been selected so that varying numbers of interference node pairs and phases at the CPA time are associated with each narrowband line. The heavy vertical lines in this figure represent the narrowband lines and the light solid curves the contours of the interference minima.*

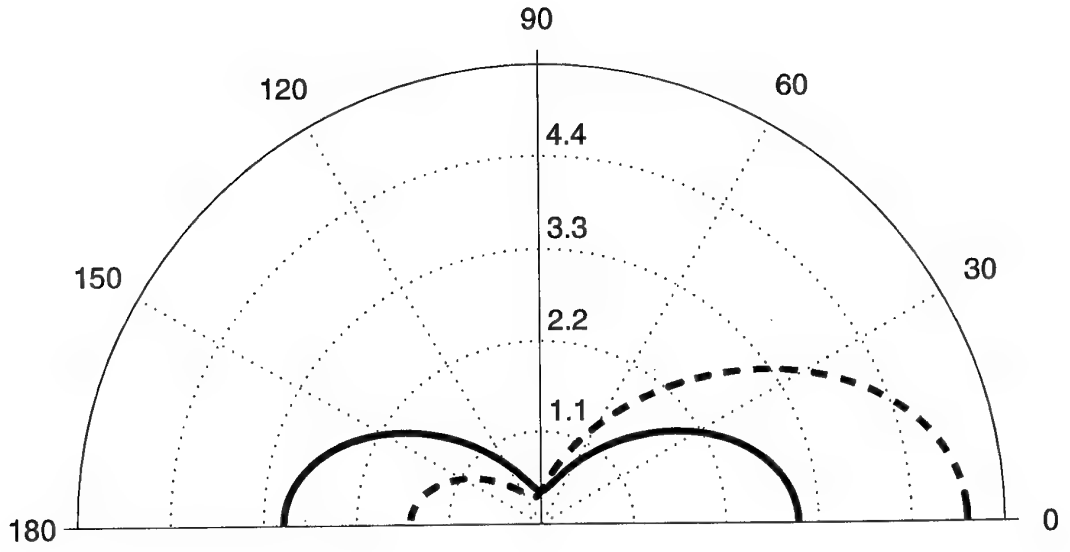

Figure 8 *Polar plots of the beam pattern relative intensities used with the current simulations. The heavy solid curve shows the symmetric dipole pattern, with the heavy dashed curve corresponding to the asymmetric dipole pattern.*

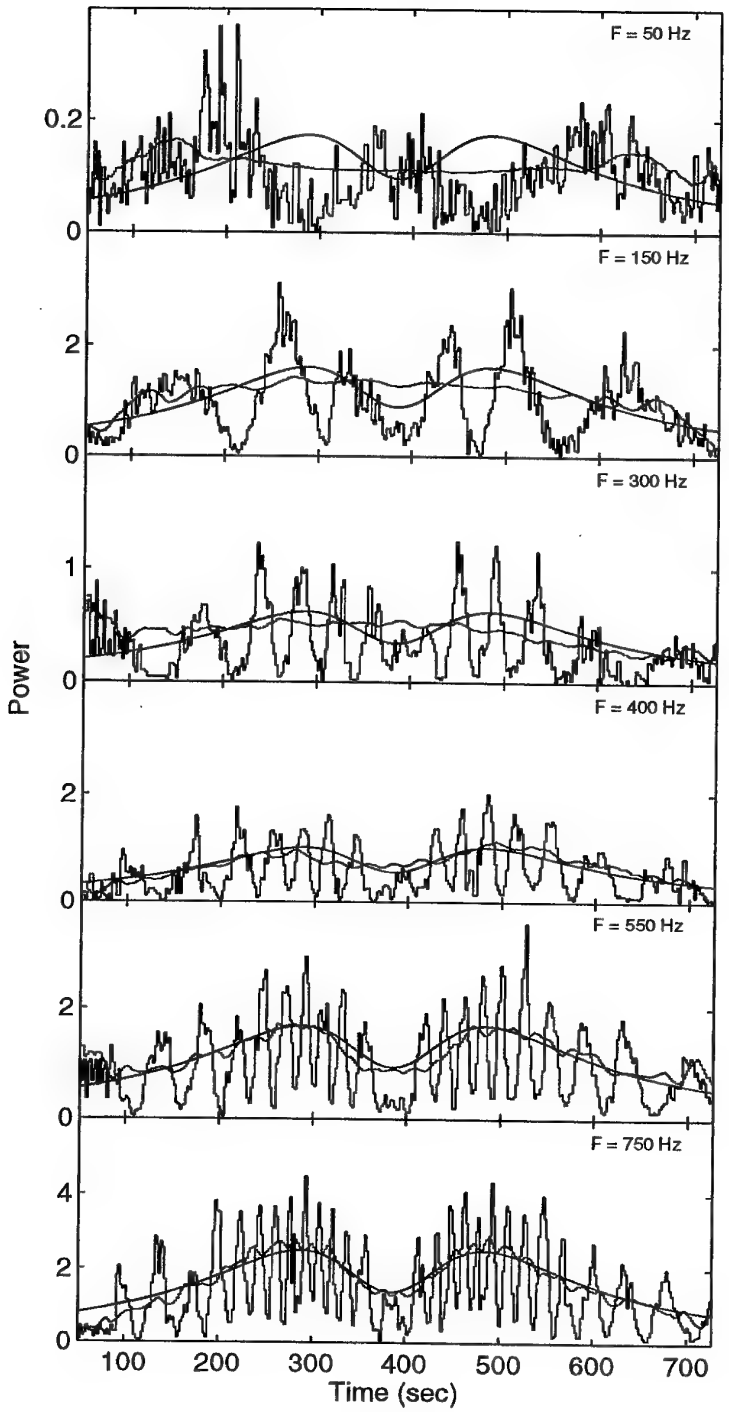

Figure 9a *The effect of smoothing on the line profiles for the six narrowband lines. This figure is for the symmetric dipole beam pattern. The red curve shows the modelled line profile, whilst the purple curve shows the profile estimated from the smoothing filter. The 50 Hz beam pattern is poorly reproduced. The quality of the match improves as the number of node pairs in the line profile is increased. In each case the smoothing window was four times the estimated interference fringe spacing.*

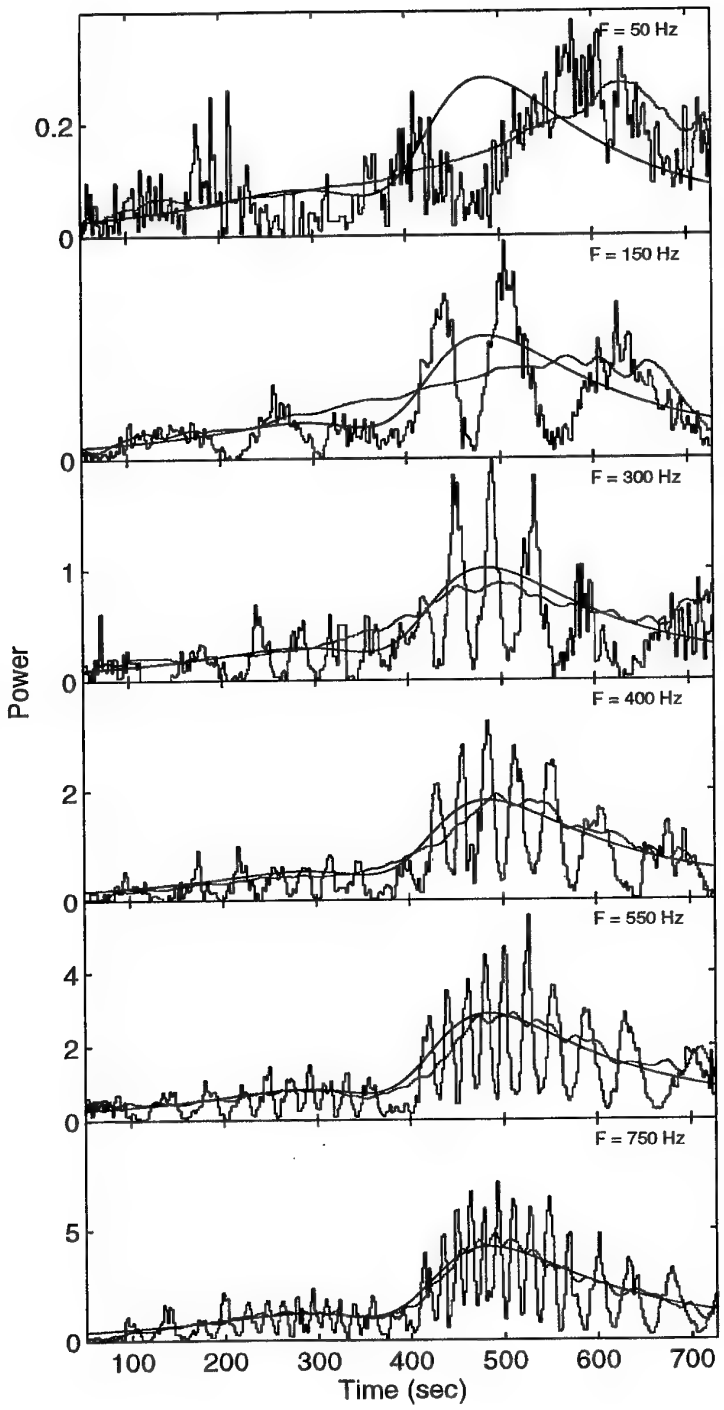

Figure 9b *The effect of smoothing on the line profiles for the six narrowband lines. This figure is for the asymmetric dipole beam pattern. The red curve shows the modelled line profile, whilst the purple curve shows the profile estimated from the smoothing filter. The 50 Hz beam pattern is poorly reproduced. The quality of the match improves as the number of node pairs in the line profile is increased. In each case the smoothing window was four times the estimated interference fringe spacing.*

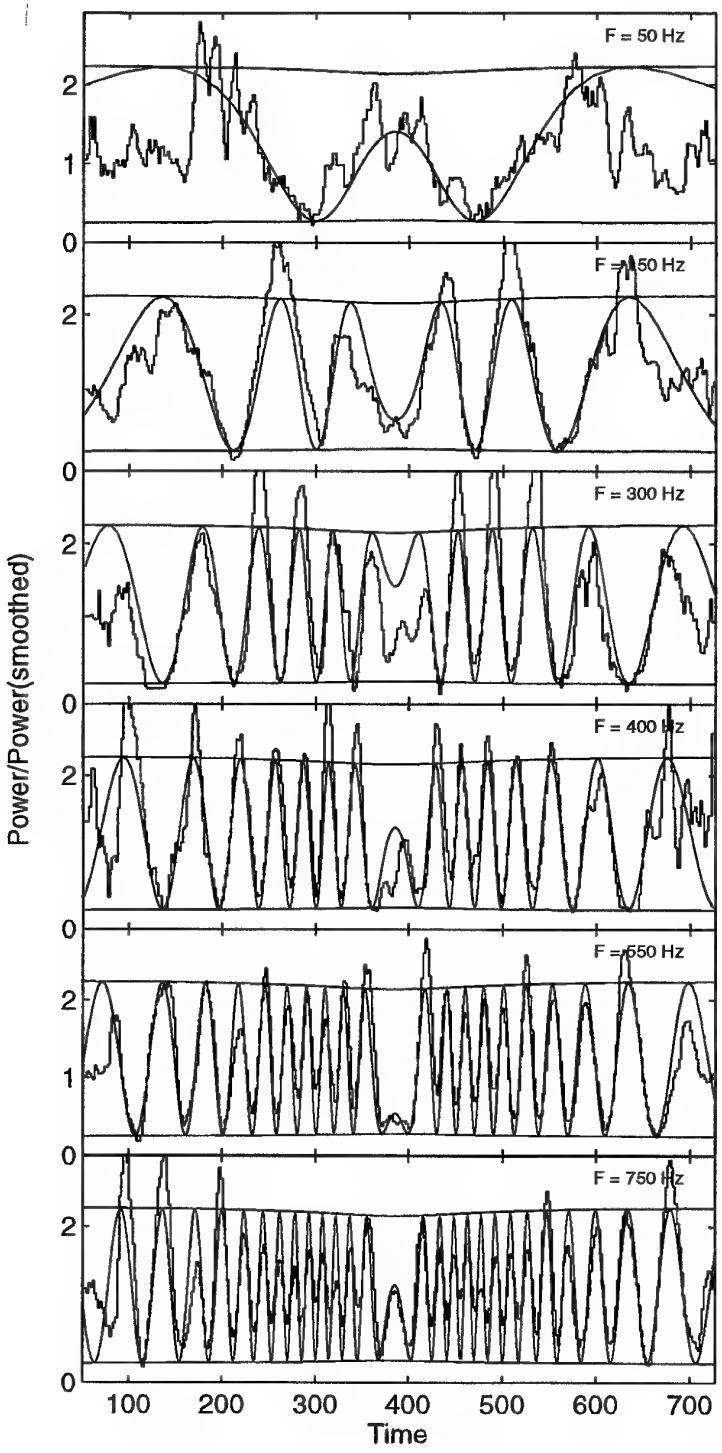

Figure 10a *The modulation functions deduced from the symmetric dipole pattern data shown in figure 9a. The patterns for this and asymmetric dipole patterns in figure 10b are similar, showing that the effect of the beam pattern has been removed. The purple curve shows the modelled modulation function.*

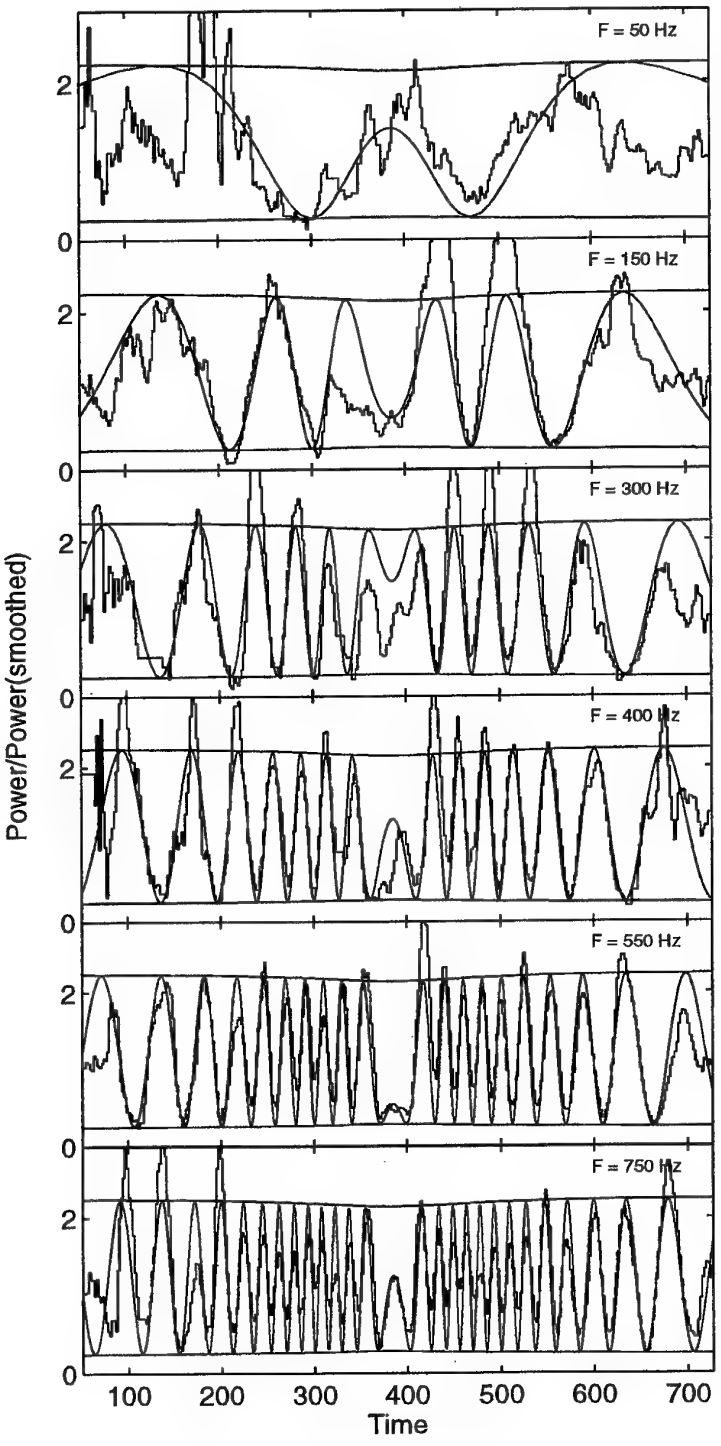

Figure 10b *The modulation functions deduced from the asymmetric dipole pattern data shown in figure 9b. The patterns for this and symmetric dipole patterns in figure 10a are similar, showing that the effect of the beam pattern has been removed. The purple curve shows the modelled modulation function.*

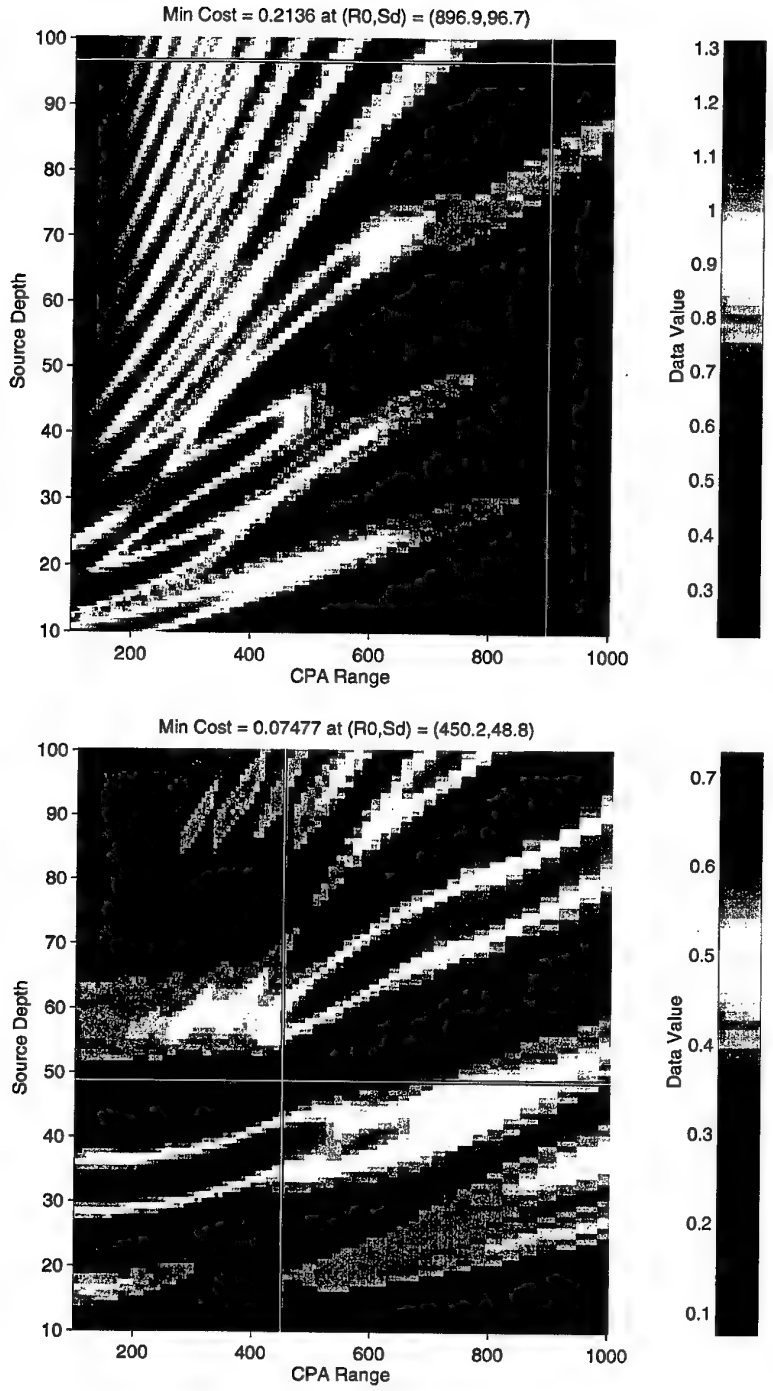

Figure 11a *The least squares cost function surfaces for a single narrowband line of 150 Hz. The data is for the symmetric dipole beam pattern. The upper figure does not include any data weighting. The lower figure includes data weighting. The weighted cost function surface shows a smoother variation and the minimum point matches the correct solution minimum. The unweighted surface is more complex, and in this example wrongly identifies the solution minimum.*

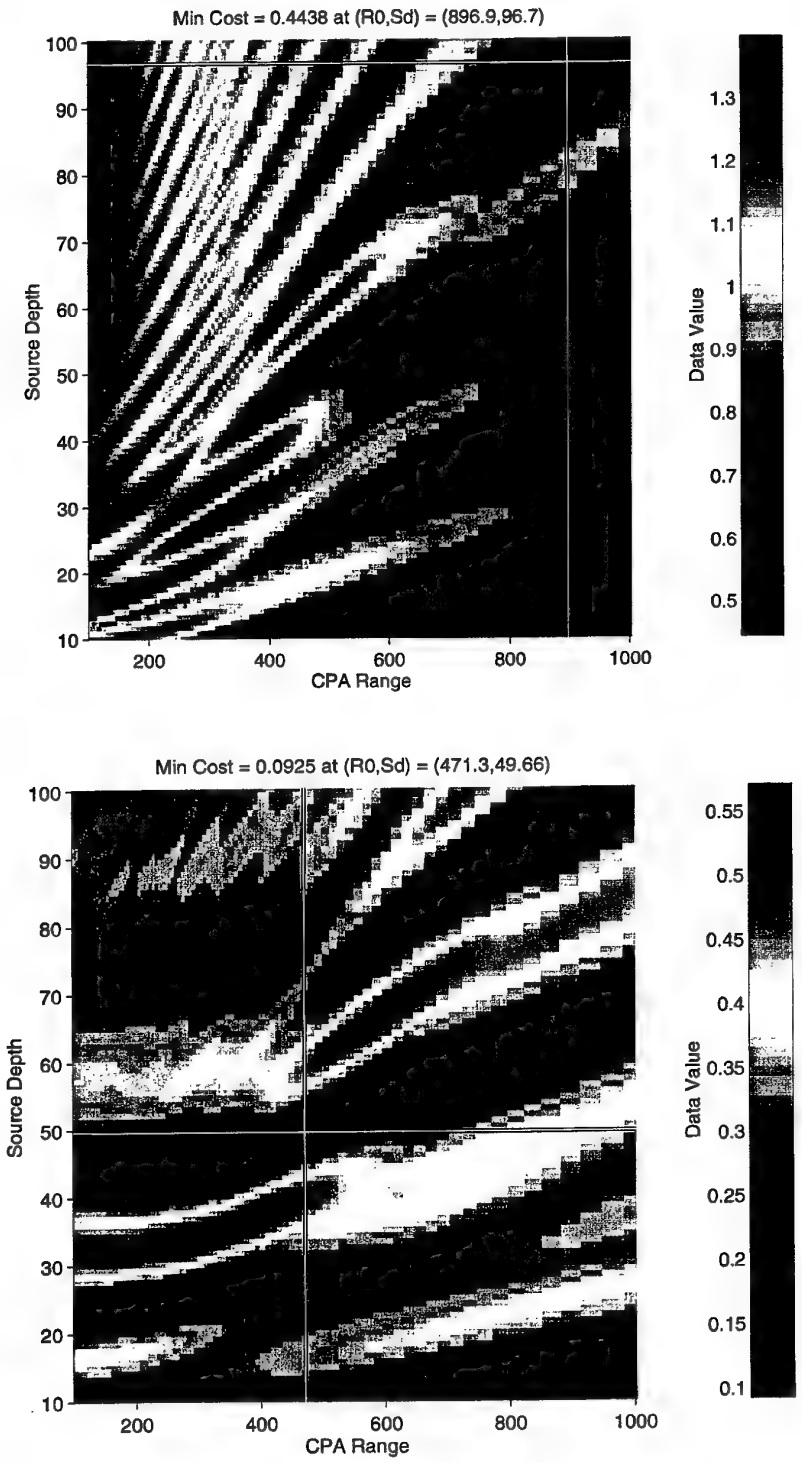

Figure 11b *The least squares cost function surfaces for a single narrowband line of 150 Hz. The data is for the asymmetric dipole beam pattern. The upper figure does not include any data weighting. The lower figure includes data weighting. These figures are similar to those in figure 11a.*

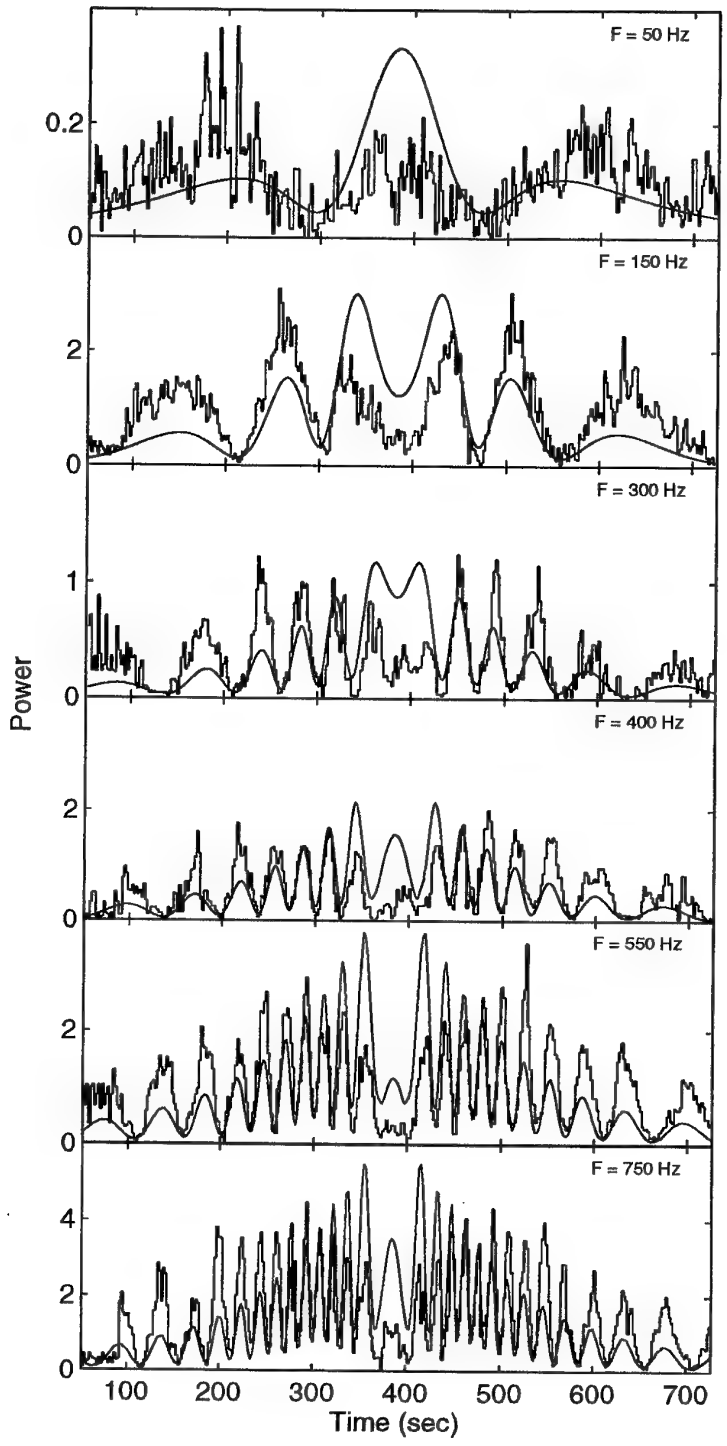

Figure 12 *The result of a global weighted least squares minimisation of the fit to the symmetric dipole data. The six narrowband lines at frequencies of 50, 150, 300, 400, 550 and 750 Hz were included in the optimisation. A direct simplex searching algorithm was used. The initial point was taken from the minimum identified in figure 11a. The estimated solution point is at* $(R_0, Sd, \eta) = (476.2, 49.9, 0.457)$, *in comparison with the true point at (477, 50, 0.5).*

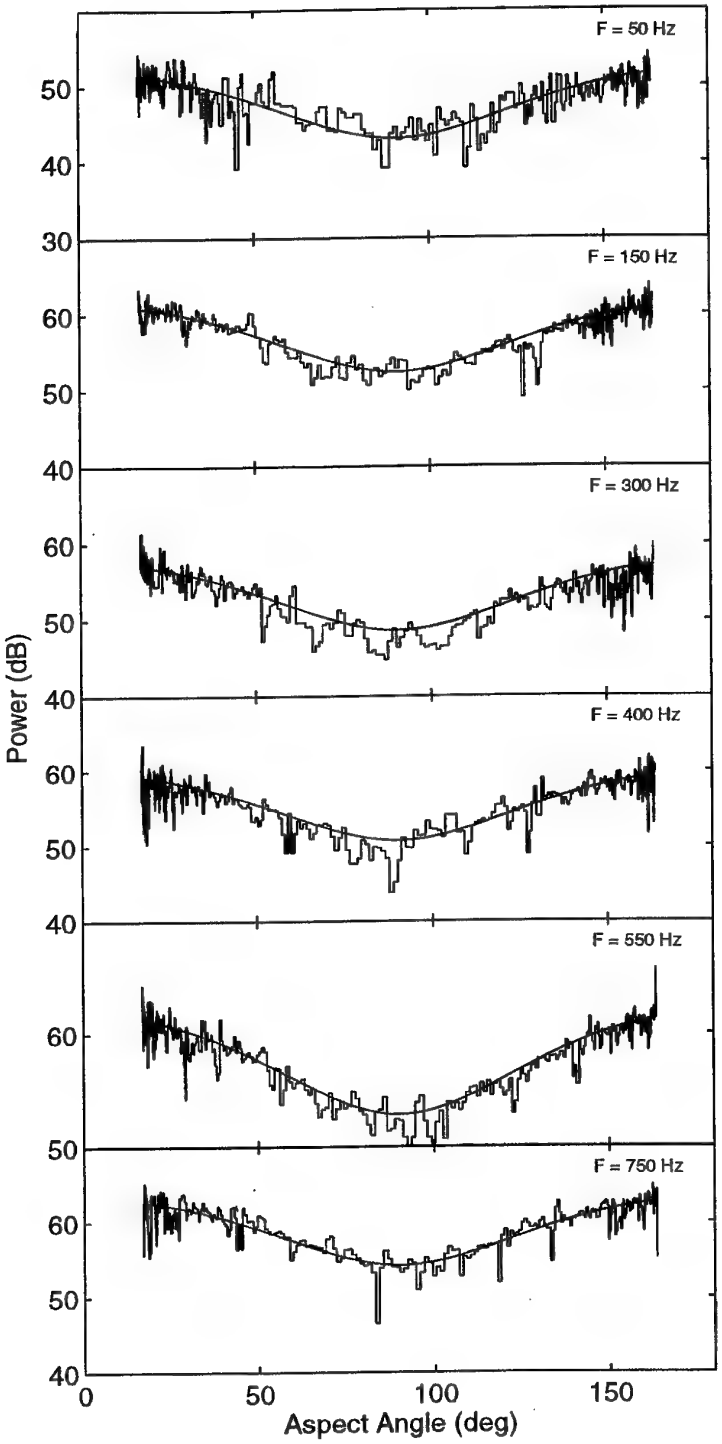

Figure 13 *The estimated beam patterns for the six data sets of figure 12. The pattern should be identical in shape in each case. The red curve shows the true beam pattern. These have been normalised to the data since no calibration of the data was included. Good agreement in the true and extracted line shapes is obtained in each case.*

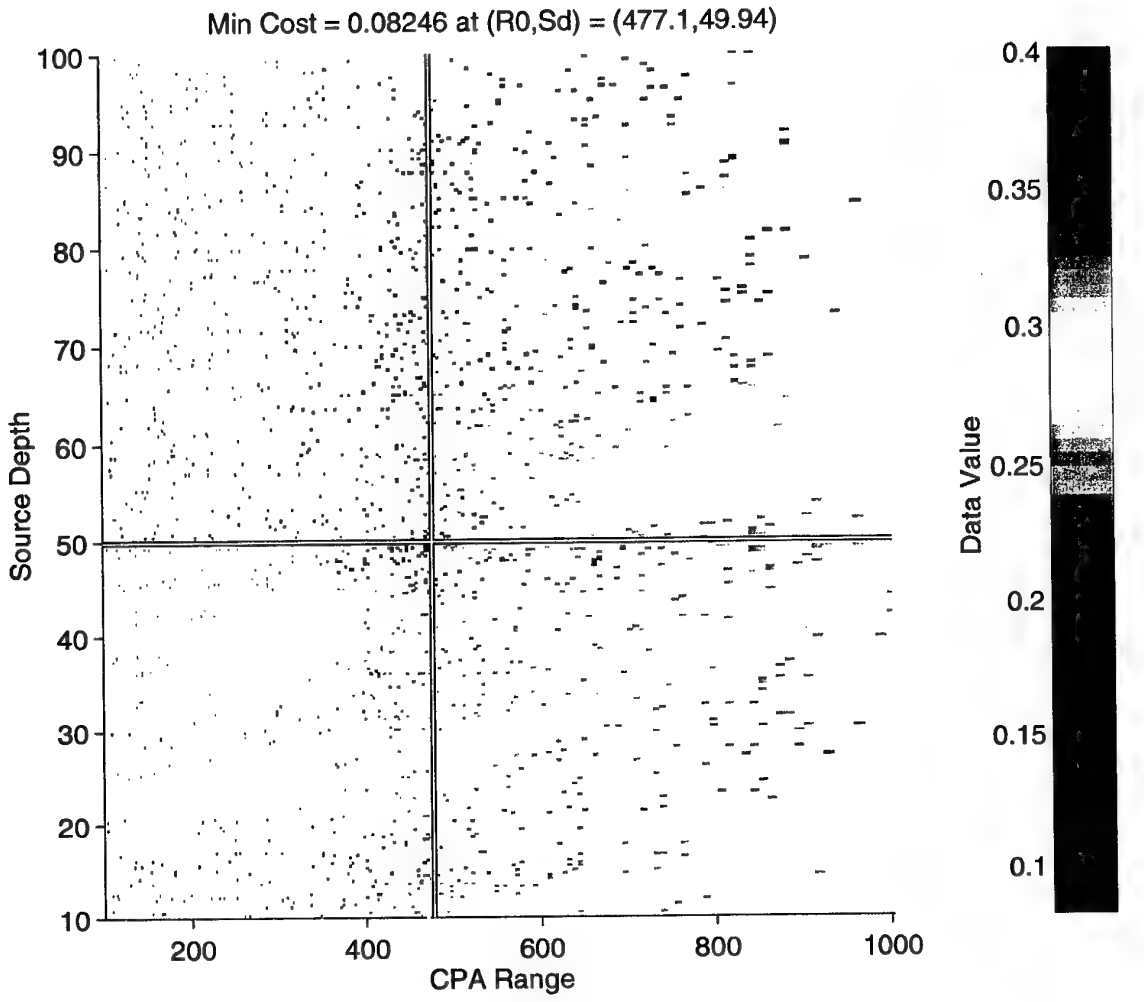

Figure 14 *The sampled weighted least squares cost function as produced using the simulated annealing algorithm. The correct minimum point is identified. The statistics on this optimisation are given in the text. The standard annealing parameters described in Appendix A were used. Approximately 2% of the available grid has been evaluated. This figure shows how the entire range has been sampled, but that the region closest to the solution point has received the more detailed inspection.*

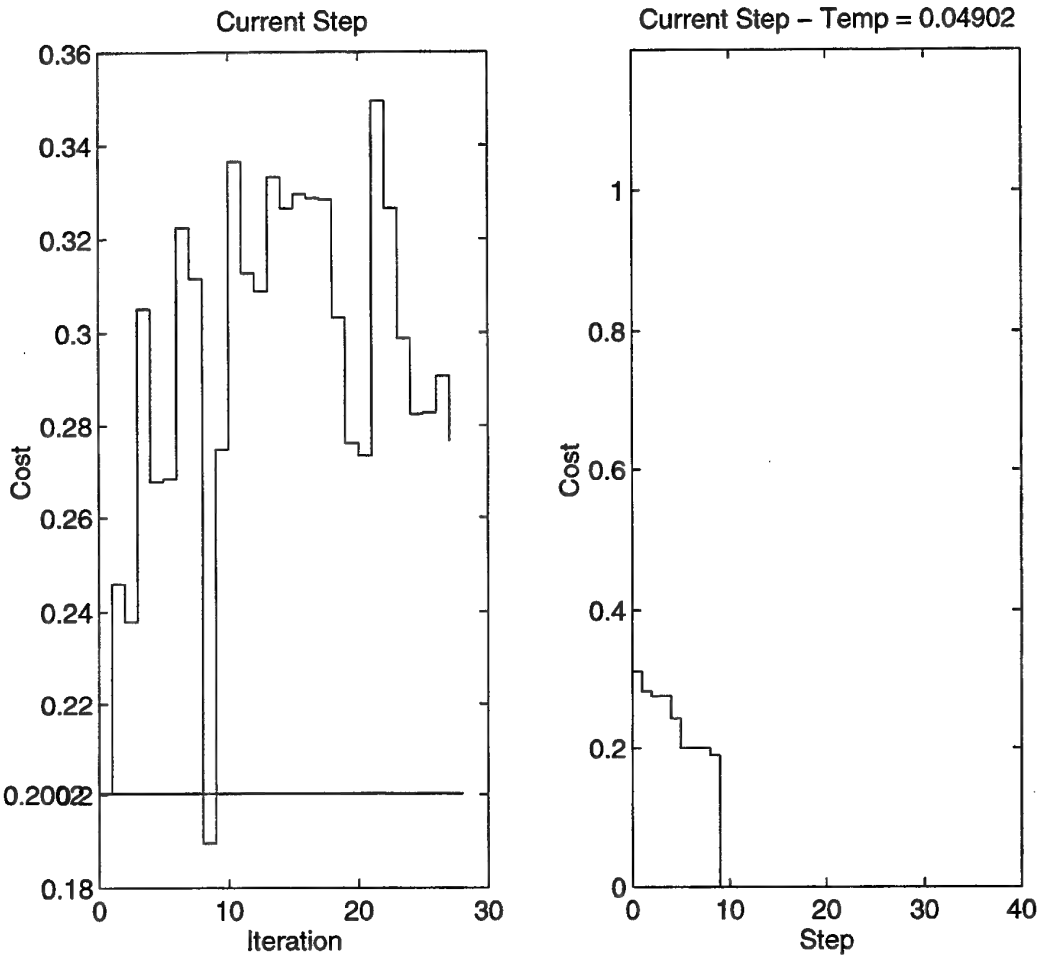

Figure 15 *A snapshot of the simulated annealing search. This figure shows the progress made at the eighth cycle of the search. The left figure shows the sample cost function values for the current cycle, with the horizontal line indicating the current best cost function value. A better solution point has been identified. The right curve shows the progress in the best cost function value with cycle number.*

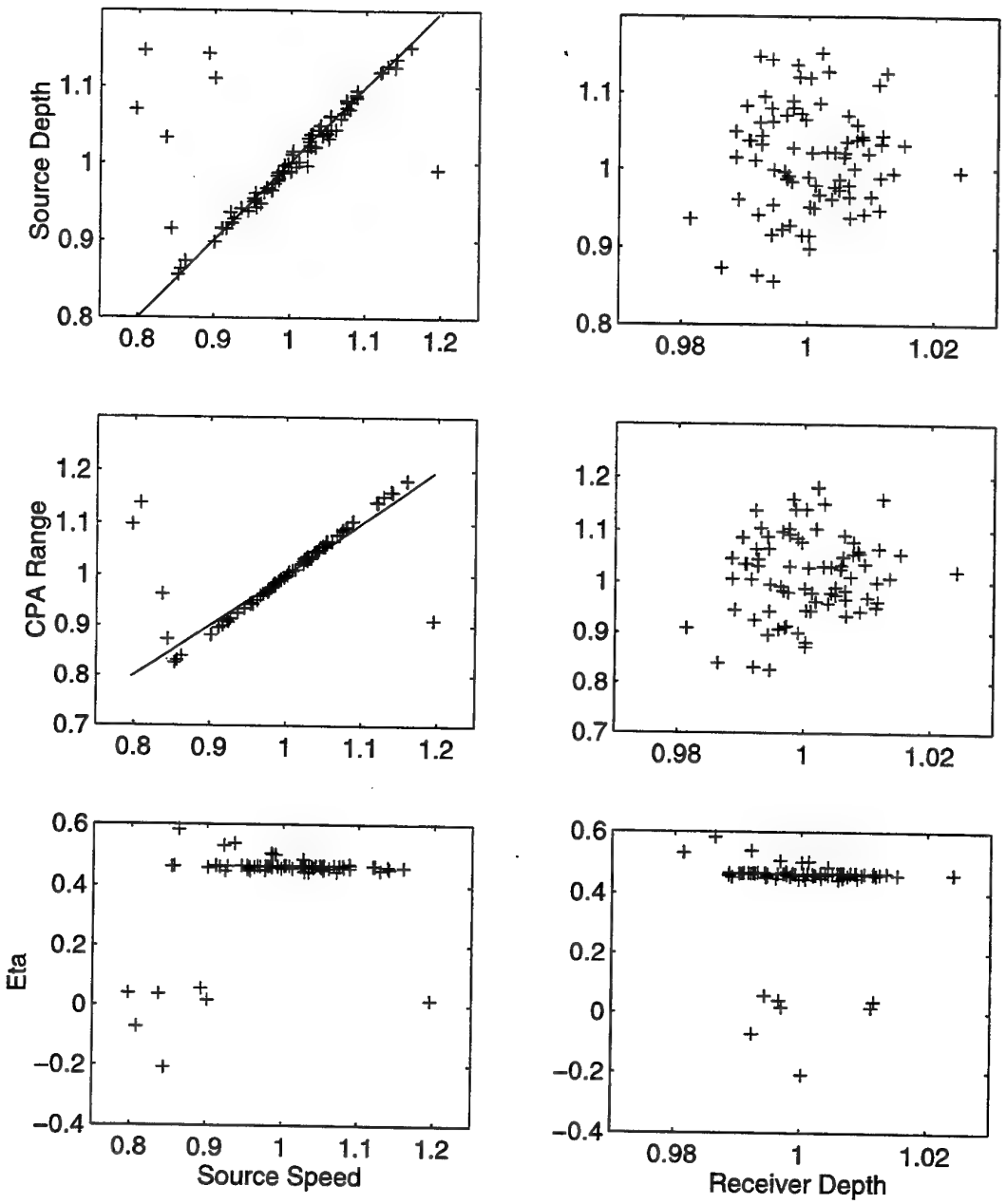

Figure 16 *Correlations between the various trajectory parameters obtained from a variational study. The left column shows the variation of the deduced unknown parameters with the known source speed. The right column shows the variation with the known receiver depth. The data are normalised to the true values given in the text. The solid curves indicate the expected correlation based on equation 17. The source depth and CPA range appear to be strongly dependent on the source speed. The reflection coefficient is independent of the geometric parameters.*

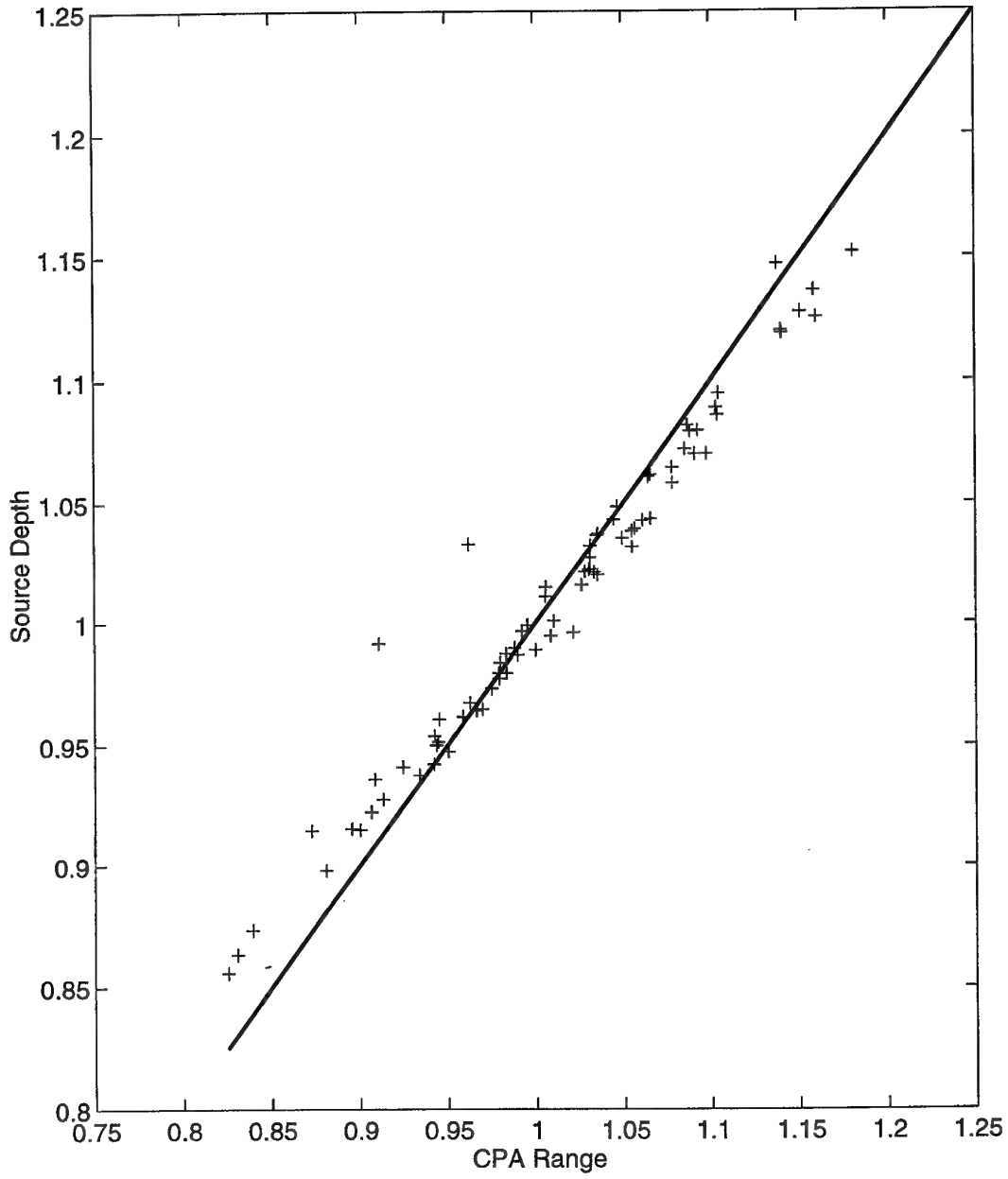

Figure 17 *The variation in the estimated solution point with changes in the known receiver depth and source speed. The data are presented relative to the true values. The solid curve shows the dependence expected from equation 17. The large change in the solution point matches the large change imposed on the source speed (±15%).*

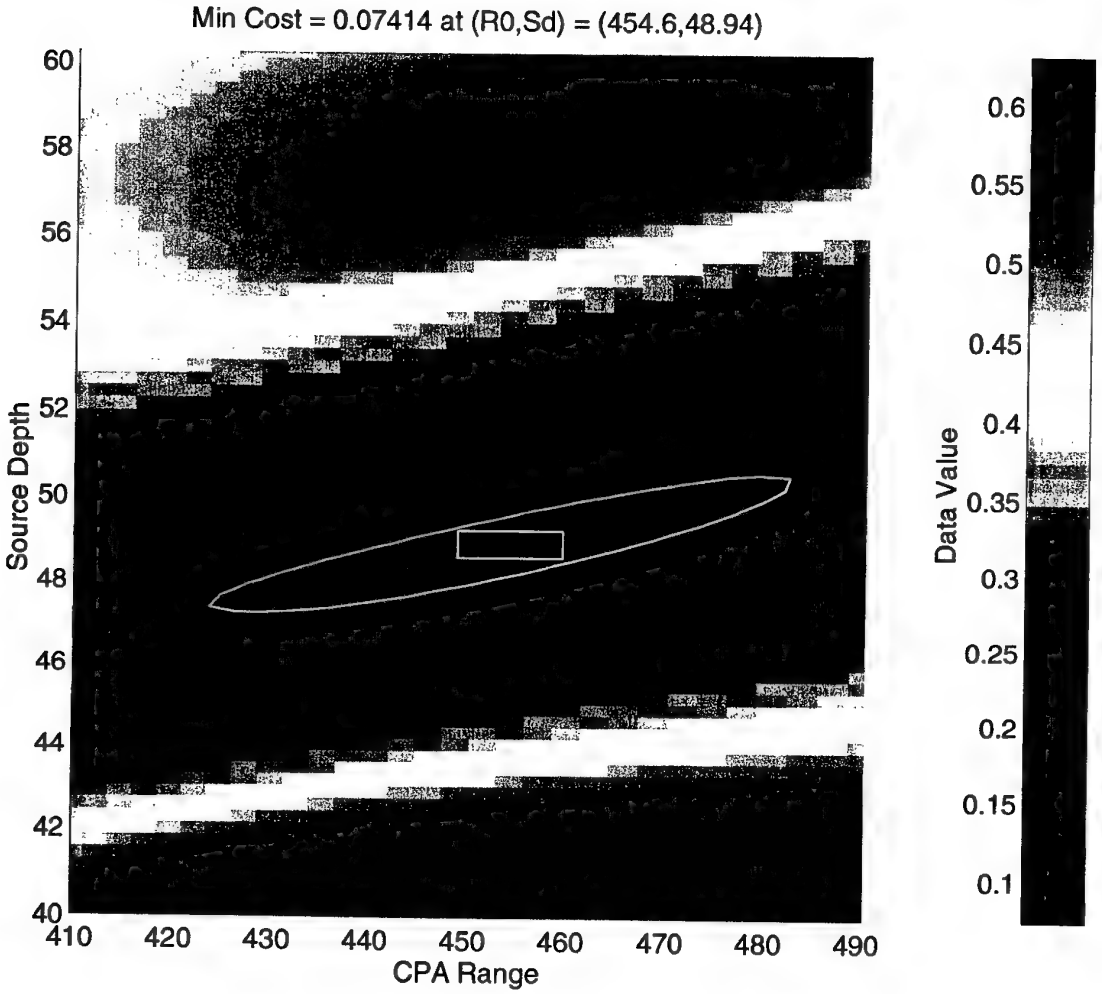

Figure 18 *Estimated error bounds on the solution point for the symmetric dipole beam pattern. The data for the single narrowband line at 150 Hz were included. The figure shows the weighted cost function. The single contour represents the 95% confidence level based on equation 18. The rectangular box shows the independent uncertainty 95% confidence bounds, based on the linear least squares approximation given in equations 19–22.*

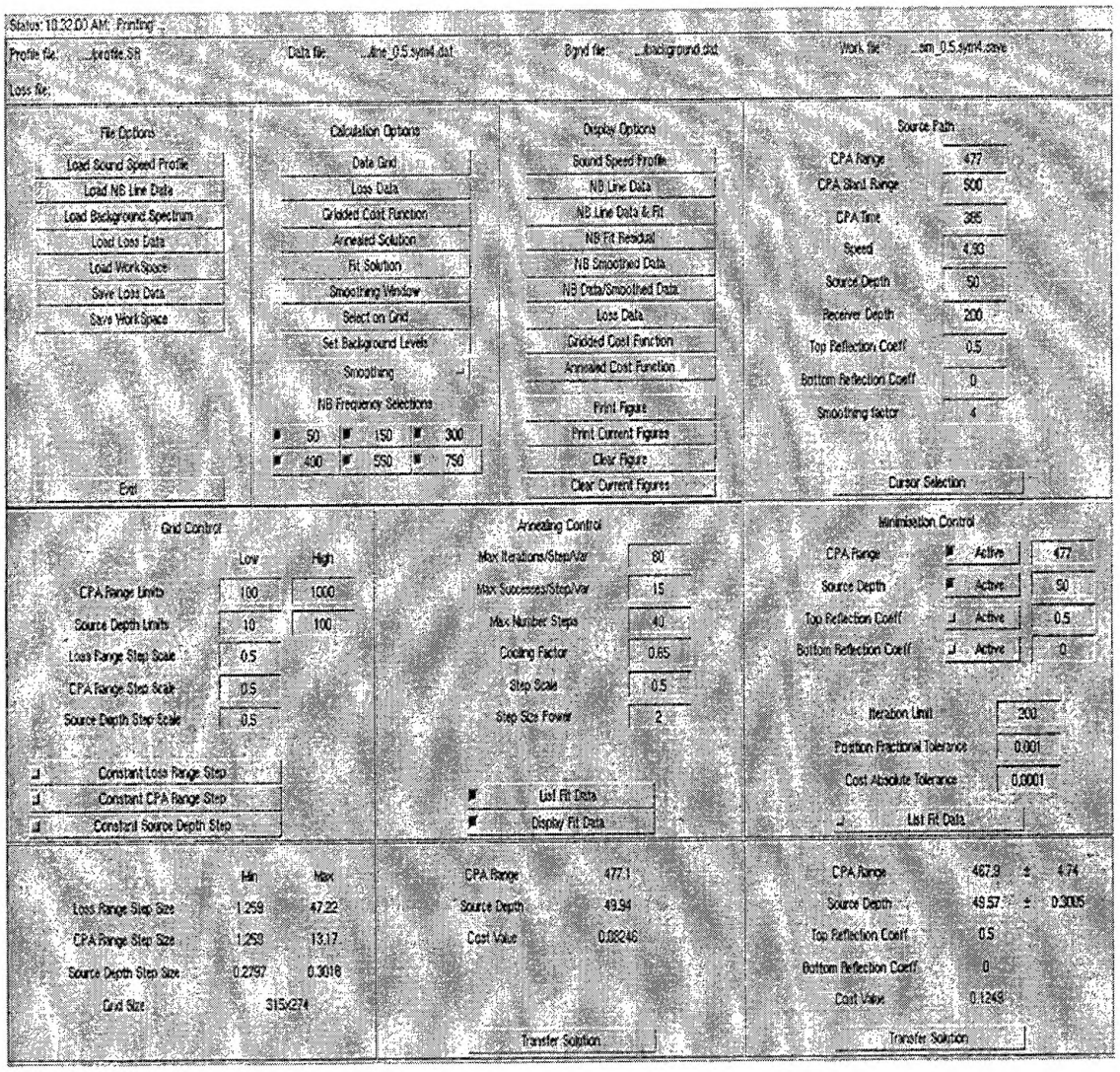

Figure B1 *The LINAL MATLAB demonstration interface. The various control buttons and options are described in Appendix B.*

DISTRIBUTION LIST

Source Localisation using Lloyd's Mirror Fringes on Narrowband Lines

Paul R. Lewis

AUSTRALIA

DEFENCE ORGANISATION

Task Sponsor

CO AJAAC, HMAS ALBATROSS, Nowra NSW 2450

S&T Program

Chief Defence Scientist
FAS Science Policy
AS Science Corporate Management
} shared copy

Director General Science Policy Development
Counsellor Defence Science, London (Doc Data Sheet)
Counsellor Defence Science, Washington (Doc Data Sheet)
Scientific Adviser to MRDC Thailand (Doc Data Sheet)
Director General Scientific Advisers and Trials/Scientific Adviser Policy and Command (shared copy)
Navy Scientific Adviser
Scientific Adviser - Army (Doc Data Sheet and distribution list)
Air Force Scientific Adviser
Director Trials

Aeronautical and Maritime Research Laboratory

Director
Chief of Maritime Operations Division
Research Leader, Sonar Technology and Processing
C.L. Davis
D. McMahon
P.R. Lewis

DSTO Library

Library Fishermens Bend
Library Maribyrnong
Library Salisbury (2 copies)
Australian Archives
Library, MOD, Pyrmont
Library, MOD, HMAS Stirling

Capability Development Division

Director General Maritime Development
Director General Land Development (Doc Data Sheet only)
Director General C3I Development (Doc Data Sheet only)

Navy

SO (Science), Director of Naval Warfare, Maritime Headquarters Annex, Garden Island, NSW 2000 (Doc Data Sheet)

Army

ABCA Office, G-1-34, Russell Offices, Canberra (4 copies)

Intelligence Program

DGSTA Defence Intelligence Organisation

Corporate Support Program (libraries)

OIC TRS, Defence Regional Library, Canberra
Officer in Charge, Document Exchange Centre (DEC), 1 copy
*US Defence Technical Information Centre, 2 copies
*UK Defence Research Information Center, 2 copies
*Canada Defence Scientific Information Service, 1 copy
*NZ Defence Information Centre, 1 copy
National Library of Australia, 1 copy

UNIVERSITIES AND COLLEGES

Australian Defence Force Academy
Library
Head of Aerospace and Mechanical Engineering
Deakin University, Serials Section (M list), Deakin University Library, Geelong, 3217
Senior Librarian, Hargrave Library, Monash University
Librarian, Flinders University

OTHER ORGANISATIONS

S. William Cumpston, Ebor Computing, 8 Ebor Av. Mile End, Adelaide, SA 5031
NASA (Canberra)
AGPS

OUTSIDE AUSTRALIA

ABSTRACTING AND INFORMATION ORGANISATIONS

INSPEC: Acquisitions Section Institution of Electrical Engineers
Library, Chemical Abstracts Reference Service
Engineering Societies Library, US
Materials Information, Cambridge Scientific Abstracts, US
Documents Librarian, The Center for Research Libraries, US

INFORMATION EXCHANGE AGREEMENT PARTNERS

Acquisitions Unit, Science Reference and Information Service, UK
Library - Exchange Desk, National Institute of Standards and Technology, US

SPARES (10 copies)

Total number of copies: **60**

DEFENCE SCIENCE AND TECHNOLOGY ORGANISATION
DOCUMENT CONTROL DATA

1. PRIVACY MARKING/CAVEAT (OF DOCUMENT)

2. TITLE

Source Localisation using Lloyd's Mirror Fringes on Narrowband Lines

3. SECURITY CLASSIFICATION (FOR UNCLASSIFIED REPORTS THAT ARE LIMITED RELEASE USE (L) NEXT TO DOCUMENT CLASSIFICATION)

Document	(U)
Title	(U)
Abstract	(U)

4. AUTHOR(S)

Paul R. Lewis

5. CORPORATE AUTHOR

Aeronautical and Maritime Research Laboratory
PO Box 4331
Melbourne Vic 3001 Australia

6a. DSTO NUMBER	6b. AR NUMBER	6c. TYPE OF REPORT	7. DOCUMENT DATE
DSTO-TR-0583	AR-010-366	Technical Report	October 1997

8. FILE NUMBER	9. TASK NUMBER	10. TASK SPONSOR	11. NO. OF PAGES	12. NO. OF REFERENCES
510/207/0792	92/259	CO AJAAC	63	6

13. DOWNGRADING/DELIMITING INSTRUCTIONS

none

14. RELEASE AUTHORITY

Chief, Maritime Operations Division

15. SECONDARY RELEASE STATEMENT OF THIS DOCUMENT

Approved for public release

OVERSEAS ENQUIRIES OUTSIDE STATED LIMITATIONS SHOULD BE REFERRED THROUGH DOCUMENT EXCHANGE CENTRE, DIS NETWORK OFFICE, DEPT OF DEFENCE, CAMPBELL PARK OFFICES, CANBERRA ACT 2600

16. DELIBERATE ANNOUNCEMENT

No Limitations

17. CASUAL ANNOUNCEMENT Yes

18. DEFTEST DESCRIPTORS

auditory localisation, narrowband, least squares, annealing

19. ABSTRACT

The analysis of the Lloyd's mirror interference of multiple narrowband lines from a sound source obtained with a single sensor is considered. A straightforward global least squares optimisation is discussed. The analysis is based on a straight line trajectory model of the source motion, and is configured for any range independent propagating medium. Two methods are proposed, each being based on a discrete optimisation on a predefined parameter grid. These are a simulated annealing algorithm and a guided search method. The least squares cost function is defined in a manner independent of the intrinsic shape of each narrowband emission. Simulation data based on an iso-speed sound profile are used to explore the proposed analysis.